REVIEW SUMMARY

ELECTROCHEMISTRY

Combining theory and experiment in electrocatalysis: Insights into materials design

Zhi Wei Seh, Jakob Kibsgaard, Colin F. Dickens, Ib Chorkendorff, Jens K. Nørskov, Thomas F. Jaramillo*

BACKGROUND: With a rising global population, increasing energy demands, and impending climate change, major concerns have been raised over the security of our energy future. Developing sustainable, fossil-free pathways to produce fuels and chemicals of global importance could play a major role in reducing carbon dioxide emissions while providing the feedstocks needed to make the products we use on a daily basis. One prospective goal is to develop electrochemical conversion processes that can convert molecules in the atmosphere (e.g., water, carbon dioxide, and nitrogen) into higher-value products (e.g., hydrogen, hydrocarbons, oxygenates, and ammonia) by coupling to renewable energy. Electrocatalysts play a key role in these energy conversion technologies because they increase the rate, efficiency, and selectivity of the chemical transformations involved. Today's electrocatalysts, however, are inadequate. The grand challenge is to develop advanced electrocatalysts with the enhanced performance needed to enable widespread penetration of clean energy technologies.

ADVANCES: Over the past decade, substantial progress has been made in understanding several key electrochemical transformations, particularly those that involve water, hydrogen, and oxygen. The combination of theoretical and experimental studies working in concert has proven to be a successful strategy in this respect, yielding a framework to understand catalytic trends that can ultimately provide rational guidance toward the development of improved catalysts. Catalyst design strategies that aim to increase the number of active sites and/or increase the intrinsic activity of each active site have been successfully developed. The field of hydrogen evolution, for example, has seen important breakthroughs over the years in the development of highly active non–precious metal catalysts in acid. Notable advancements have also been made in the design of oxygen reduction and evolution catalysts, although there remains substantial room for improvement. The combination of theory and experiment elucidates the remaining challenges in developing further improved catalysts, often involving scaling relations among reactive intermediates. This understanding serves as an initial platform to design strategies to circumvent technical obstacles, opening up opportunities and approaches to develop higher-performance electrocatalysts for a wide range of reactions.

ON OUR WEBSITE

Read the full article at http://dx.doi.org/10.1126/science.aad4998

OUTLOOK: A systematic framework of combining theory and experiment in electrocatalysis helps to uncover broader governing principles that can be used to understand a wide variety of electrochemical transformations. These principles can be applied to other emerging and promising clean energy reactions, including hydrogen peroxide production, carbon dioxide reduction, and nitrogen reduction, among others. Although current paradigms for catalyst development have been helpful to date, a number of challenges need to be successfully addressed in order to achieve major breakthroughs. One important frontier, for example, is the development of both experimental and computational methods that can rapidly elucidate reaction mechanisms on broad classes of materials and in a wide range of operating conditions (e.g., pH, solvent, electrolyte). Such efforts would build on current frameworks for understanding catalysis to provide the deeper insights needed to fine-tune catalyst properties in an optimal manner. The long-term goal is to continue improving the activity and selectivity of these catalysts in order to realize the prospects of using renewable energy to provide the fuels and chemicals that we need for a sustainable energy future. ■

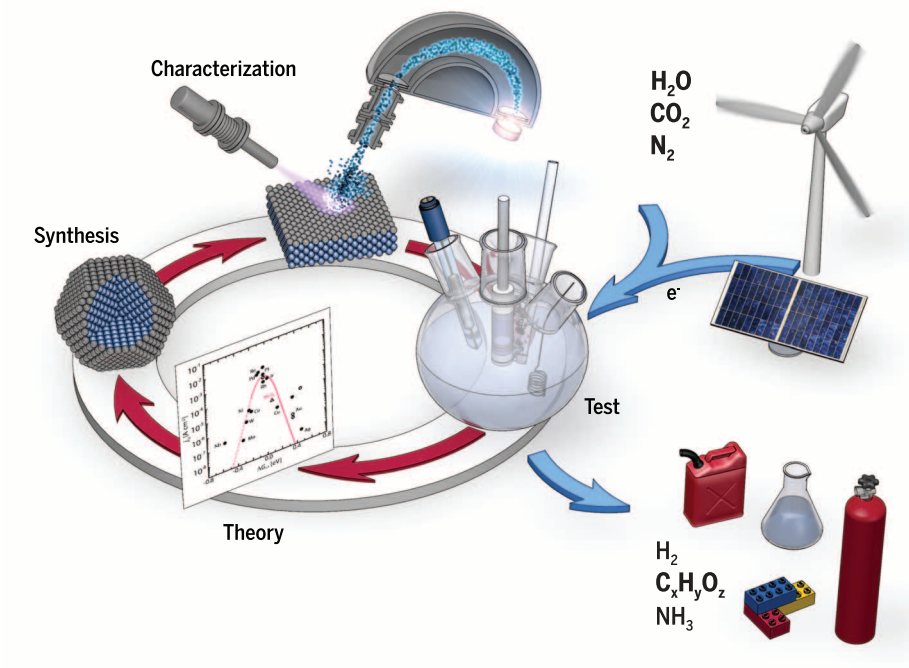

Electrochemical energy conversion. Schematic showing electrochemical conversion of water, carbon dioxide, and nitrogen into value-added products (e.g., hydrogen, hydrocarbons, oxygenates, and ammonia), using energy from renewable sources. The combination of theoretical and experimental studies working in concert provides us with insight into these electrochemical transformations and guides the development of the high-performance electrocatalysts needed to enable these technologies.

The list of author affiliations is available in the full article online.
*Corresponding author. Email: jaramillo@stanford.edu
Cite this article as Z. W. Seh *et al.*, *Science* **355**, eaad4998 (2017). DOI: 10.1126/science.aad4998

REVIEW

ELECTROCHEMISTRY

Combining theory and experiment in electrocatalysis: Insights into materials design

Zhi Wei Seh,[1,2,3] Jakob Kibsgaard,[1,2,4] Colin F. Dickens,[1,2] Ib Chorkendorff,[4] Jens K. Nørskov,[1,2] Thomas F. Jaramillo[1,2]*

Electrocatalysis plays a central role in clean energy conversion, enabling a number of sustainable processes for future technologies. This review discusses design strategies for state-of-the-art heterogeneous electrocatalysts and associated materials for several different electrochemical transformations involving water, hydrogen, and oxygen, using theory as a means to rationalize catalyst performance. By examining the common principles that govern catalysis for different electrochemical reactions, we describe a systematic framework that clarifies trends in catalyzing these reactions, serving as a guide to new catalyst development while highlighting key gaps that need to be addressed. We conclude by extending this framework to emerging clean energy reactions such as hydrogen peroxide production, carbon dioxide reduction, and nitrogen reduction, where the development of improved catalysts could allow for the sustainable production of a broad range of fuels and chemicals.

Creating a global-scale sustainable energy system for the future while preserving our environment is one of the most crucial challenges facing humanity today (*1*–*3*). According to the International Energy Agency, global energy demand reached 18 TW in 2013, the vast majority (~80%) of which was derived from fossil resources (coal, oil, and gas) (*4*). With a growing world population and expanding industrialization, global energy demand is projected to further increase from 18 TW in 2013 to 24 or 26 TW in 2040 under the "new policies" or "current policies" scenarios, respectively, with a corresponding rise in carbon dioxide emissions from 32 Gt year^{-1} in 2013 to 37 or 44 Gt year^{-1} in 2040 (*4*). As a result, major concerns have been raised over the energy supply, particularly in regard to climate change associated with the use of fossil fuels. Thus, a serious impetus exists to diversify our energy sources, reducing our reliance on fossil fuels by turning to renewable energy such as solar, wind, and hydroelectric power.

Greater penetration of renewable electricity is important, as overall the electricity sector accounts for approximately 12% of global energy demand (2.1 out of 17.6 TW in 2010) (*5*). Other key energy sectors requiring the development of sustainable pathways include transportation and the chemical industry. In 2010, transportation accounted for 19% (3.3 TW) of global energy (*5*). Although approximately 43% (1.4 TW) of transportation energy demand involved light-duty vehicles, where electrification is already playing a role to help decarbonize the system, the remaining 57% (1.9 TW) was used for commercial transportation—marine, aviation, rail, and heavy-duty road vehicles—where electrification is much more challenging (*5*). Projections indicate that energy demand for light-duty transportation will likely remain relatively flat in the coming decades; however, energy use for commercial transportation is projected to grow by approximately two-thirds between 2010 and 2040, from 1.9 to 3.2 TW (*5*). Because chemical fuels are a more natural fit for this sector, there is strong interest in the development of sustainable pathways to such fuels.

Similarly, the current energy demand for the production of industrial chemicals in 2010 was 8% (1.5 TW) of global energy, almost all of which was derived from fossil fuels (*5*). To meet worldwide demand for products such as plastics and fertilizers, energy use in the chemical industry is also expected to rise by about two-thirds between 2010 and 2040, to 2.5 TW (*5*). A sustainable, fossil fuel–free path to producing industrial chemicals of global importance, such as hydrogen (50 Mt year^{-1}), hydrogen peroxide (2.2 Mt year^{-1}), ethylene (115 Mt year^{-1}), propylene (73 Mt year^{-1}), methanol (40 Mt year^{-1}), and ammonia (175 Mt year^{-1}), could play a substantial role in reducing carbon dioxide emissions while providing the chemicals needed to make the products used globally on a daily basis (*6*–*8*).

Figure 1 shows possible sustainable pathways for the production of important fuels and chemicals, including hydrogen, hydrocarbons, oxygenates, and ammonia, by either replacing or working in concert with conventional energy production. Earth's atmosphere provides a universal feedstock of water, carbon dioxide, and nitrogen, which can potentially be converted into the aforementioned products via electrochemical processes coupled to renewable energy if electrocatalysts with the required properties can

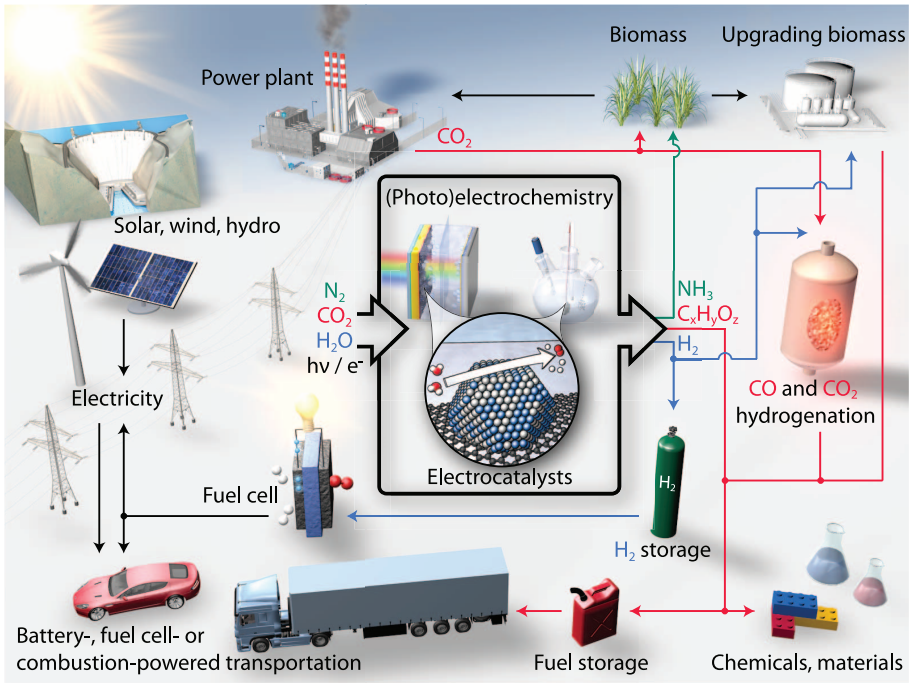

Fig. 1. Sustainable energy future. Schematic of a sustainable energy landscape based on electrocatalysis.

[1]SUNCAT Center for Interface Science and Catalysis, Department of Chemical Engineering, Stanford University, Stanford, CA 94305, USA. [2]SUNCAT Center for Interface Science and Catalysis, SLAC National Accelerator Laboratory, Menlo Park, CA 94025, USA. [3]Institute of Materials Research and Engineering, Agency for Science, Technology and Research (A*STAR), Innovis, 138634 Singapore. [4]Department of Physics, Technical University of Denmark, DK-2800 Kongens Lyngby, Denmark.
*Corresponding author. Email: jaramillo@stanford.edu

be developed. For instance, the water-splitting reaction, which consists of the hydrogen and oxygen evolution half-reactions, has attracted great attention as a sustainable source of hydrogen (*9*, *10*). Hydrogen is an attractive energy carrier that can be used to produce clean electricity in fuel cells, where the hydrogen oxidation and oxygen reduction reactions convert chemical energy into electrical energy (*11*, *12*). Hydrogen peroxide, an essential chemical in the pulp- and paper-bleaching and water treatment industries, can potentially be derived from the oxygen reduction reaction (ORR) as well (*13*). Carbon dioxide captured from the atmosphere or directly from point sources could become a feedstock for fuels, commodity chemicals, fine chemicals, and precursors to polymers and plastics via preliminary electroreduction (*14*). Likewise, the electroreduction of nitrogen to ammonia would allow for the production of fertilizers sustainably and locally at the point of application and at the required concentration, eliminating distribution costs stemming from the inflexibly large-scale, centralized Haber-Bosch process (*15*). Crucial to enabling this vision is the development of improved electrocatalysts with the appropriate efficiency and selectivity for the chemical transformations involved.

There are generally two strategies to improve the activity (or reaction rate) of an electrocatalyst system: (i) increasing the number of active sites on a given electrode (e.g., through increased loading or improved catalyst structuring to expose more active sites per gram) or (ii) increasing the intrinsic activity of each active site (*10*). These strategies (Fig. 2) are not mutually exclusive and can ideally be addressed simultaneously, leading to the greatest improvements in activity. At the same time, there are physical limits to how much catalyst material can be loaded onto an electrode without affecting other important processes, such as charge and mass transport (*10*). For this reason, Fig. 2 shows a plateau effect observed in practice at high catalyst loadings. On the other hand, increasing intrinsic activity leads to direct increases in electrode activity in a manner that mitigates transport issues arising from high catalyst loadings; with improved intrinsic activity, the catalyst loading can be decreased, which also saves on catalyst costs. Moreover, catalyst activity is measured across many orders of magnitude; the difference in intrinsic activity between a good catalyst and a poor catalyst can be more than 10 orders of magnitude, whereas the difference between a high-loading and a low-loading catalyst might only be one to three orders of magnitude (*10*).

The field of electrocatalysis has seen much progress in recent years, as evidenced by the rapidly increasing number of publications on this subject. This review focuses on several quintessential case studies of electrocatalysis for different energy conversion reactions, surveying state-of-the-art catalyst materials and using theory as a means to rationalize trends in performance. By examining multiple reactions involving water, hydrogen, and oxygen, we describe a framework that reveals broader trends in electrocatalysis for clean energy conversion.

We begin by presenting theoretical results with a focus on understanding catalytic trends using a descriptor-based approach: a framework that aims to establish a select few, key properties of a catalyst surface that are necessary but possibly not sufficient for high activity. We describe how this relatively fast, simple, and straightforward approach has been implemented successfully in recent years to develop advanced catalysts. The next major step would be to extend the modeling capabilities to capture greater complexities regarding the catalyst and the electrode-electrolyte interface in a manner that does not require excessive time and resources. Developing modeling approaches that use minimal resources to rapidly and accurately predict reaction mechanisms and rate data across a broad range of catalyst materials and reaction conditions represents an important aim for future work. The same holds true for the development of more advanced experimental methods that are capable of providing atomic- and molecular-scale depictions of the electrode-electrolyte interface under operating conditions. At this point, we can provide a description of current theoretical approaches to further these types of insights (e.g., on reaction rates and mechanisms) with more detailed calculations performed using microkinetic models. The combination of the descriptor-based approach to cover a broad set of systems coupled to detailed studies of single systems has proven fruitful. Future efforts to advance both theory and experiment will allow for a more detailed picture of catalysis on surfaces.

Hydrogen evolution/oxidation reactions

Active catalysts are required to minimize the overpotential necessary to drive the hydrogen evolution reaction (HER; $2H^+ + 2e^- \rightarrow H_2$) (*9*, *10*). The HER is a classic example of a two-electron transfer reaction with one catalytic intermediate, H* (where * denotes a site on the electrode surface), and may occur through either the Volmer-Heyrovsky or the Volmer-Tafel mechanism (*9*, *10*):

$$\text{Volmer step: } H^+ + e^- + * \rightarrow H^* \quad (1)$$

$$\text{Heyrovsky step: } H^* + H^+ + e^- \rightarrow H_2 + * \quad (2)$$

$$\text{Tafel step: } 2H^* \rightarrow H_2 + 2* \quad (3)$$

The rate of the overall reaction is largely determined by the hydrogen adsorption free energy, ΔG_H (*16*, *17*). If hydrogen binds to the surface too weakly, the adsorption (Volmer) step will limit the overall reaction rate, whereas if the binding is too strong, the desorption (Heyrovsky/Tafel) step will limit the rate. Thus, a necessary but insufficient condition for an active HER catalyst is $\Delta G_H \approx 0$ (*16*, *17*). In plotting experimentally measured exchange current densities for a wide range of catalyst materials against ΔG_H at the appropriate coverage calculated from density functional theory (DFT), a volcano relationship emerges—a quantitative illustration of the so-called Sabatier principle (Fig. 3A) (*18*–*20*). An active catalyst binds reaction intermediate(s) neither too strongly nor too weakly. Understanding how to control binding energies of reactive intermediates on a surface is the key to designing materials with improved performance. The volcano shown in Fig. 3A is the first of several described in this work, each representing a different electrochemical reaction, and represents a broader framework by which catalysts across a wide range of chemical reactions can be viewed.

Although these volcanoes provide insight into the optimum catalyst for a given class of catalyst materials, there are additional factors not present in the simple descriptor-based model that are needed to quantitatively determine absolute reaction rates—for instance, variations in the size of kinetic barriers from one class of materials to the next. This is why MoS_2 is observed to have lower exchange current densities than the precious metals shown in Fig. 3A, even though it has a ΔG_H value near the optimum. Kinetic barriers can also change as a function of pH for a given potential versus the reversible hydrogen electrode (RHE), which results in an observed pH dependence of current density (*21*). Despite possible variations in the processes involved (e.g., regarding pH or kinetic barriers), we note that the activity volcano does not shift left or right, but rather only up and down, meaning that the descriptor still serves its purpose of identifying the binding characteristics of optimal HER catalysts (*22*). However, for a full quantitative understanding of these effects, more detailed and efficient methods of calculating electrochemical barriers are required for proton transfer reactions involving both hydroxide and hydronium ions (*20*, *23*–*28*), an important goal for future modeling efforts.

Platinum sits very near the top of the hydrogen volcano, with an almost thermo-neutral ΔG_H, and is well known as the best-performing catalyst for the HER, requiring negligible overpotentials to achieve high reaction rates in acidic solutions (Fig. 3, B and C) (*10*). However, the scarcity and high cost of Pt could limit its widespread technological use. This has sparked a search for Earth-abundant catalysts that potentially could replace Pt—a search where the development of MoS_2-based HER catalysts serves as an excellent example of theory-guided discovery and design of new electrocatalysts (*10*).

For decades, MoS_2 was believed to be inactive for the HER (*29*). However, inspired by hydrogen-producing enzymes such as hydrogenases and nitrogenases in nature, DFT calculations were performed on the Mo($10\bar{1}0$) edge of MoS_2, revealing that at 50% hydrogen coverage, it possesses a ΔG_H of 0.08 eV, near the optimal value of 0 eV (Fig. 3A) (*30*). In stark contrast, the basal plane exhibits a ΔG_H of 1.92 eV, which explains the poor activity of bulk MoS_2 crystals (*31*). These calculations led to the synthesis of MoS_2 on a carbon black support to expose the edge sites and its subsequent examination in a membrane electrode assembly setup (*30*). A geometric area–normalized current density of 10 mA cm^{-2}_{geo} was achieved at ~175 mV overpotential, which at the time was the most active non–precious metal HER catalyst reported in acid.

Soon after, it was confirmed experimentally that the edges of MoS_2 are indeed the catalytic active sites for the HER (*32*). Upon depositing a single monolayer of MoS_2 nanoparticles on a Au(111) surface, the nanoparticle areas and edge lengths were measured using scanning tunneling microscopy, and the HER activity was found to scale linearly with MoS_2 perimeter length and not with MoS_2 surface area (Fig. 3, B and D). The combination of theoretical and experimental studies provided the key insight that only the MoS_2 edges are active, thereby motivating the development of MoS_2 catalysts with a substantial fraction of exposed edge sites.

One promising approach to achieving this exposure is by nanostructuring the MoS_2 catalysts (Fig. 2). To this end, a three-dimensional mesoporous MoS_2 nanostructure with a double-gyroid morphology was explored (Fig. 3D) (*33*). The nanoscale curvature of the double-gyroid structure minimizes the formation of extended basal planes, exposing a high density of active edge sites. As a result, the turnover frequency averaged across all surface sites (TOF_{avg}) of double-gyroid MoS_2 exceeded that of MoO_3-MoS_2 nanowires prepared using a similar sulfidation technique by a factor of 2 to 4 (Fig. 3D) (*33*, *34*). A shortcoming of the double-gyroid structure, however, was the long electron transport distance from the active site to the conductive substrate, which led to increased resistive loss because the electron mobility perpendicular to MoS_2 basal planes is lower than the in-plane electron mobility by about three orders of magnitude (*10*). In an attempt to alleviate this problem, vertically aligned MoS_2 nanostructures were synthesized, which not only exposed a large number of edge sites at the surface but also enabled facile electron transport to the conductive substrate (Fig. 3D) (*35*, *36*).

Another attractive approach in catalyst development is to disperse nanoparticles on supports with high surface area (Fig. 2). For instance, MoS_2 nanoparticles were prepared on reduced graphene oxide (RGO) nanosheets (*37*). Relative to the RGO-free synthesis, use of the RGO support led to better dispersion and reduced aggregation of MoS_2 nanoparticles, resulting in superior activity due to an increased number of edge sites and enhanced charge transport (Fig. 3B).

Intercalation of lithium ions into the van der Waals gap of MoS_2 has also been investigated as a means to increase the HER activity by tuning the electronic properties of MoS_2 (Fig. 2) (*38*–*40*). Lithium intercalation leads to chemical exfoliation of MoS_2 and a phase transition from the 2H semiconducting polymorph to the 1T metallic polymorph, another means to engineer catalyst activity (Figs. 2 and 3D). It was suggested that the enhanced activity of 1T-MoS_2 over similarly prepared 2H-MoS_2 was due to an increase in the number of active edge sites, as well as a decrease in the charge transfer resistance (*38*). Another study further proposed that the edges of 1T-MoS_2 were not the main active sites and that the basal plane could be catalytically active instead (*39*). Most recently, it was shown that vacancies in the MoS_2 basal plane also exhibit high activity that can be tuned by straining the MoS_2 sheets (*41*).

Amorphous molybdenum sulfide has also been shown to possess high HER activity, primarily due to its high surface area (Fig. 3D). Amorphous molybdenum sulfides can be prepared using electrodeposition (*42*) or wet chemical synthesis (*43*) without any thermal treatment, which makes them attractive for certain applications where avoiding high-temperature sulfidation is desired—for example, in the fabrication of photoelectrochemical devices. The composition of the as-synthesized amorphous molybdenum sulfide materials was determined to be close to MoS_3, but upon applying reducing potentials in an electrochemical cell, the surface transformed to MoS_2, as evidenced by in situ studies (*43*, *44*). Amorphous molybdenum sulfides can be further doped with transition metals such as Fe, Co, and Ni, improving their activity substantially (*45*). Under acidic conditions, the improvement was largely due to an increase in surface area, whereas TOF_{avg} was improved in neutral conditions.

The extensive engineering of MoS_2-based catalysts over the years to increase the number of active sites has been remarkable, but their overall electrode activity is still limited, as generally only a small fraction of sites (edge sites) contribute to the reaction rate (Fig. 3, B to D) (*10*, *32*). This has led to the design of molecular clusters with undercoordinated sulfur at the surface that resemble the edges of MoS_2, such as $[Mo_3S_4]^{4+}$ cubanes (*46*, *47*), Mo^{IV}-disulfide (*48*), and thiomolybdate $[Mo_3S_{13}]^{2-}$ complexes (*49*) (Fig. 3D). Further loading of catalyst material is another means of increasing the number of active sites, but such an approach would eventually result in limitations from mass and/or charge transport (Fig. 2). This has spurred the development of other catalysts with higher intrinsic activity, leveraging the theoretical framework of a descriptor based on $\Delta G_H \approx 0$. These include transition metal phosphides (*50*–*59*), selenides (*60*), borides (*61*), carbides (*61*, *62*), and nitrides (*63*), some of which exhibit HER activities closer to that of Pt in terms of the overpotential to reach 10 mA cm^{-2}_{geo}. However, because of high catalyst loadings and large surface areas, the non–precious metal systems are still orders of magnitude behind Pt in terms of TOF_{avg} under acidic conditions (Fig. 3, B to D). In alkaline media, state-of-the-art non–precious metal catalysts have also been developed, some of which (e.g., Ni-Mo systems) exhibit low overpotentials to reach 10 mA cm^{-2}_{geo} (*64*–*66*). However, such systems also exhibit TOF_{avg} values that are substantially lower than that of Pt, values that are similar to those of non–precious metal systems in acid, hence leaving much room for improvement (*64*–*66*). Homogeneous catalysts with high TOF_{avg} have also been developed, although they typically require large overpotentials to reach appreciable current densities (Fig. 3B) (*67*–*69*).

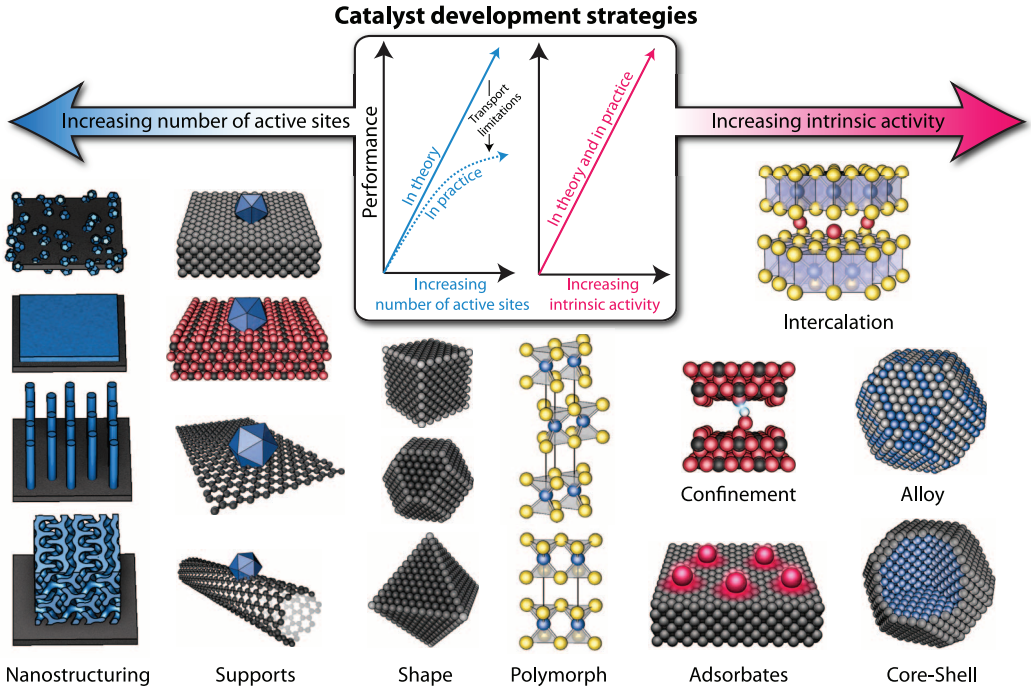

Fig. 2. Catalyst development strategies. Schematic of various catalyst development strategies, which aim to increase the number of active sites and/or increase the intrinsic activity of each active site.

Developing non–precious metal analogs to Pt for the HER in both acid and base remains an important challenge. In addition to catalyst activity, long-term stability is an equally important metric and should be reported in conjunction with activity. Helpful approaches to assessing catalyst durability include accelerated cyclic voltammetry tests, long-term stability studies that quantify the amount of catalyst leached into the electrolyte, and the use of thin-film catalyst morphologies (*10*, *66*).

The hydrogen oxidation reaction (HOR), which involves the same reaction steps as the HER except in reverse, has received much less attention in the context of non–precious metal catalyst development (*21*, *70*). According to theory, an optimal HOR catalyst should also exhibit $\Delta G_H \approx 0$ and reside at the top of the same volcano in Fig. 3A. As such, we would expect Pt to be the best pure metal catalyst for both the HER and HOR in acid, which is in fact observed experimentally (*21*, *70*). However, this is not true for MoS_2 catalysts, which show much poorer HOR activity relative to the HER (*32*). Understanding the differences between precious metal and non–precious metal catalysts for the HOR remains a frontier in research. One distinction involves coverage effects in catalysis: The ΔG_H of metallic Pt has little dependence on hydrogen coverage, whereas that of MoS_2 shows substantial variation (*31*). Surface oxidation can also play a role for some catalyst systems; for example, with non–precious metals and metal alloys, the metallic surface expected during HER conditions is quite different from the metal oxide/hydroxide surface that can form during HOR conditions (*20*). Accurately modeling expected surface structures and stoichiometries of the catalyst material during different operating conditions represents a broader challenge in catalysis. As a result, the search continues toward Earth-abundant materials with metallic conductivity and almost-invariant ΔG_H that can open up new opportunities in the design of high-performance electrocatalysts for both the HER and the HOR.

Oxygen reduction/evolution reactions

The four-electron ORR ($O_2 + 4H^+ + 4e^- \rightarrow 2H_2O$) requires improved electrocatalysts to increase its rate and efficiency (*11*, *12*). Generally, the ORR involves either four proton-electron transfers to reduce oxygen to water, desirable for fuel cells, or a two–proton-electron pathway, attractive for the production of hydrogen peroxide (see below) (*13*). The four-electron pathway can proceed via several mechanisms. A direct four-electron mechanism can either be dissociative or associative in nature, depending on the oxygen dissociation barrier on the catalyst surface (*71*). An indirect four-electron mechanism involves first the two-electron pathway to hydrogen peroxide, followed by further reduction to water (*71*):

$$\text{Dissociative: } O_2 + 2^* \rightarrow 2O^* \quad (4)$$

$$2O^* + 2H^+ + 2e^- \rightarrow 2OH^* \quad (5)$$

$$2OH^* + 2H^+ + 2e^- \rightarrow 2H_2O + 2^* \quad (6)$$

$$\text{Associative: } O_2 + ^* \rightarrow O_2^* \quad (7)$$

$$O_2^* + H^+ + e^- \rightarrow OOH^* \quad (8)$$

$$OOH^* + H^+ + e^- \rightarrow O^* + H_2O \quad (9)$$

$$O^* + H^+ + e^- \rightarrow OH^* \quad (10)$$

$$OH^* + H^+ + e^- \rightarrow H_2O + ^* \quad (11)$$

The free energies of all the above intermediates have been calculated on a variety of close-packed metal surfaces, and a volcano plot was constructed relating the theoretical ORR activity and ΔE_O, with Pt near the top (Fig. 4A) (*71*). For metals that bind oxygen too strongly, the activity is limited by proton-electron transfer to O* or OH*. On the other hand, for metals that bind oxygen too weakly, the activity is limited by proton-electron transfer to O_2* (associative mechanism) or splitting of the O-O bond in O_2 (dissociative mechanism), depending on the applied potential (*71*).

Although the volcano framework presented in Fig. 4A is similar to that discussed above for the HER/HOR in Fig. 3A, there is a substantial difference. Unlike in the case of the HER/HOR with one reaction intermediate, the four-electron ORR involves multiple intermediates (OOH*, OH*, O*), the binding energies of which are strongly correlated and cannot be decoupled easily because of scaling relations (*71*). In fact, the scaling relation $\Delta G_{OOH} = \Delta G_{OH} + 3.2 \pm 0.2$ eV was found to apply universally to both close-packed (111) and open-packed (100) facets of face-centered cubic (fcc) metals and their alloys (Fig. 4B) (*72*, *73*). As a result of this nonideal scaling between OOH* and OH*, even a catalyst calculated to be at the top of the ORR volcano plot with optimal ΔE_O will have a nonzero theoretical overpotential of 0.3 to 0.4 V (*71*–*73*). This is the origin of the observed overpotential among even the very best ORR catalysts, including the extensively studied Pt-based systems (Fig. 4C) (*74*).

In the development of Pt-based catalysts, considerable effort has been devoted to shape-controlled synthesis to tailor the ORR activities (Fig. 2). In

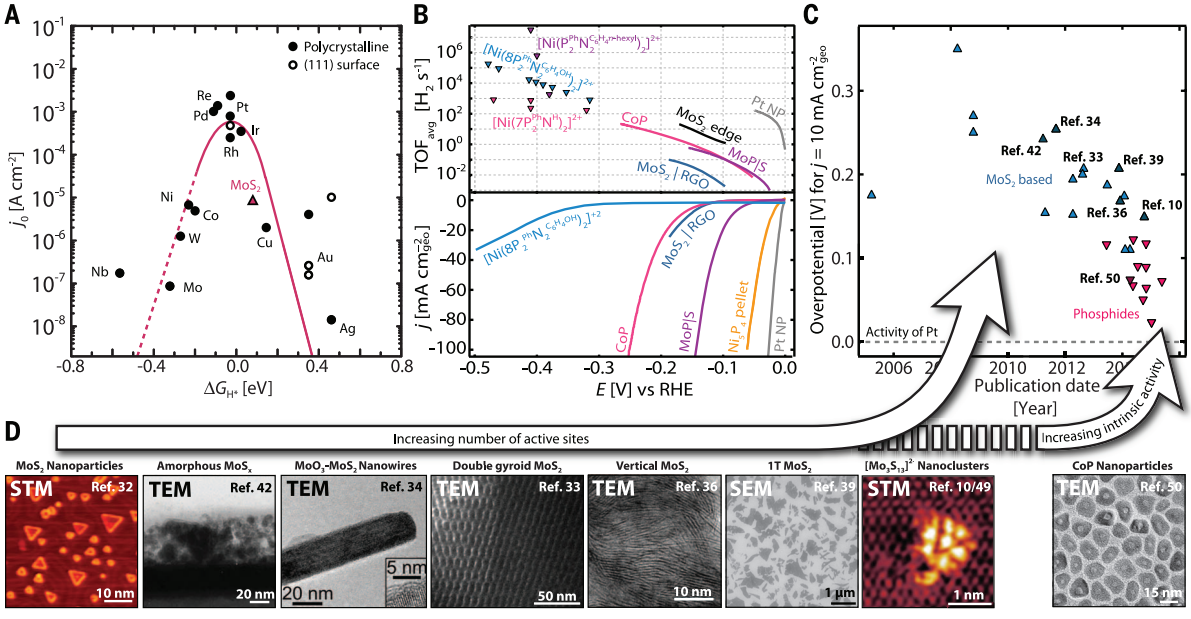

Fig. 3. The hydrogen evolution reaction. (**A**) HER volcano plot for metals and MoS_2. [Reproduced with permission from (*20*, *32*)] (**B**) TOF_{avg} plots with linear sweep voltammograms of various HER catalysts. Data obtained from (*10*, *32*, *37*, *51*, *52*, *59*). State-of-the-art Ni-based homogeneous catalysts are also included for comparison (*67*–*69*). (**C**) Chronological trend in overpotential of MoS_2-based and phosphide HER catalysts. Data obtained from (*10*, *50*–*59*) and references therein. (**D**) Representative microscopy images of HER catalysts. [Reproduced with permission from (*10*, *32*–*34*, *36*, *39*, *42*, *49*, *50*)]

nonadsorbing electrolytes such as perchloric acid, the ORR activity of low-index facets in single-crystalline Pt is known to follow the order (110) > (111) > (100) facets (*75*). When adsorbing electrolytes such as sulfuric acid are used, the (100) facets exhibit higher activity than their (111) counterparts instead, as sulfate anions strongly adsorb onto the (111) facets, blocking sites (*76*). These trends have inspired the development of Pt-based catalysts with different morphologies and exposed facets, including nanocubes (*77*), nanotubes (*78*), nanowires (*79*), nanodendrites (*80*), and nanocages (*81*) (Fig. 4D).

Support effects can also play a role in catalyst activity and stability (Fig. 2). Currently, carbon black is the most common support for Pt-based catalysts (*82*–*92*). However, the instability of carbon black under high potentials related to weak Pt-C interactions has prompted the search for more stable supports that can anchor Pt catalysts firmly, including $Ti_{0.7}Mo_{0.3}O_2$ (*93*) and tin-doped indium oxide (*94*), which have been shown to enhance catalytic activities as well.

Alloying is another extensively used strategy to enhance the ORR performance of Pt-based catalysts (Fig. 2). Alloying can decrease the oxygen adsorption energy of the top Pt layer of Pt_3M alloys (M = Ni, Fe, Co, Ti) (*95*, *96*). Pt_3Sc and Pt_3Y were predicted theoretically to be promising and stable Pt-based alloys for the ORR (*97*). This was confirmed experimentally using bulk polycrystalline Pt_3Sc and Pt_3Y catalysts; relative to pure Pt, the specific activity of the Pt_3Sc catalyst was enhanced by a factor of 1.5 to 1.8 and that of the Pt_3Y catalyst by a factor of 6 to 10 (*97*). This scheme has been expanded to include alkaline earth metals and the lanthanide series (*98*). To leverage the effects of nanostructuring, size-selected Pt_xY nanoparticles 4 to 9 nm in diameter were also prepared, the best of which exhibited a mass activity exceeding that of Pt nanoparticles by a factor of 3 (*99*). The activity of the catalysts was found to increase with decreasing average Pt-Pt distances, indicating that compressive strain exerted on the surface Pt atoms by the alloy core led to improved catalytic activity, which is supported by further studies on mass-selected Pt_xGd nanoparticles (*99*–*101*).

Another alloy found to outperform pure Pt is Pt_3Ni (*95*, *96*). Extended single-crystal surfaces of $Pt_3Ni(111)$, with a Pt-rich outermost layer caused by thermal annealing and restructuring in the near-surface region, were prepared (*102*). These so-called Pt-skin structures showed a specific activity 10 times that of Pt(111) and 90 times that of state-of-the-art Pt/C catalysts. Subsequently, three-dimensional Pt_3Ni nanoframes were synthesized from structural evolution of $PtNi_3$ polyhedra in solution (Fig. 4D) (*103*). These nanoframes with large, highly accessible surface areas exhibited improvement in specific activity and mass activity by factors of 22 and 36, respectively, relative to state-of-the-art Pt/C catalysts, even after 10,000 potential cycles. Recently, doping Pt_3Ni octahedra with transition metals was reported to further enhance their ORR activities (Fig. 4D) (*104*). In particular, doping with Mo led to improvement in specific activity and mass activity by factors of 81 and 73, respectively, relative to commercial Pt/C catalysts. Computational results indicate that Mo preferentially occupies surface vertex and edge sites in the presence of adsorbed oxygen, where it forms relatively strong Mo-Pt and Mo-Ni bonds to stabilize both Pt and Ni atoms against dissolution (*104*). Despite the notable improvement in activity, the Mo-doped Pt_3Ni system still requires ~280 mV overpotential to reach 2 mA cm^{-2}_{Pt}, which is far from the equilibrium potential for the ORR, leaving substantial opportunity for catalyst improvement (Fig. 4C).

As discussed above, Pt is the best pure metal catalyst for both the HER and HOR in acid, essentially as a result of microscopic reversibility: Both reactions involve the same steps, except in opposite directions. According to the same reasoning, one might expect Pt, which is the best pure metal ORR catalyst, to perform as well for the oxygen evolution reaction (OER); however, this is not the case observed experimentally (*105*). One reason is that microscopic reversibility only holds for a process taking place close to equilibrium. When large overpotentials are needed to drive the reaction in the two directions, the requirements for catalysis in each direction could be substantially different (*106*). In addition, at the high positive potentials required for the OER, metals including Pt generally

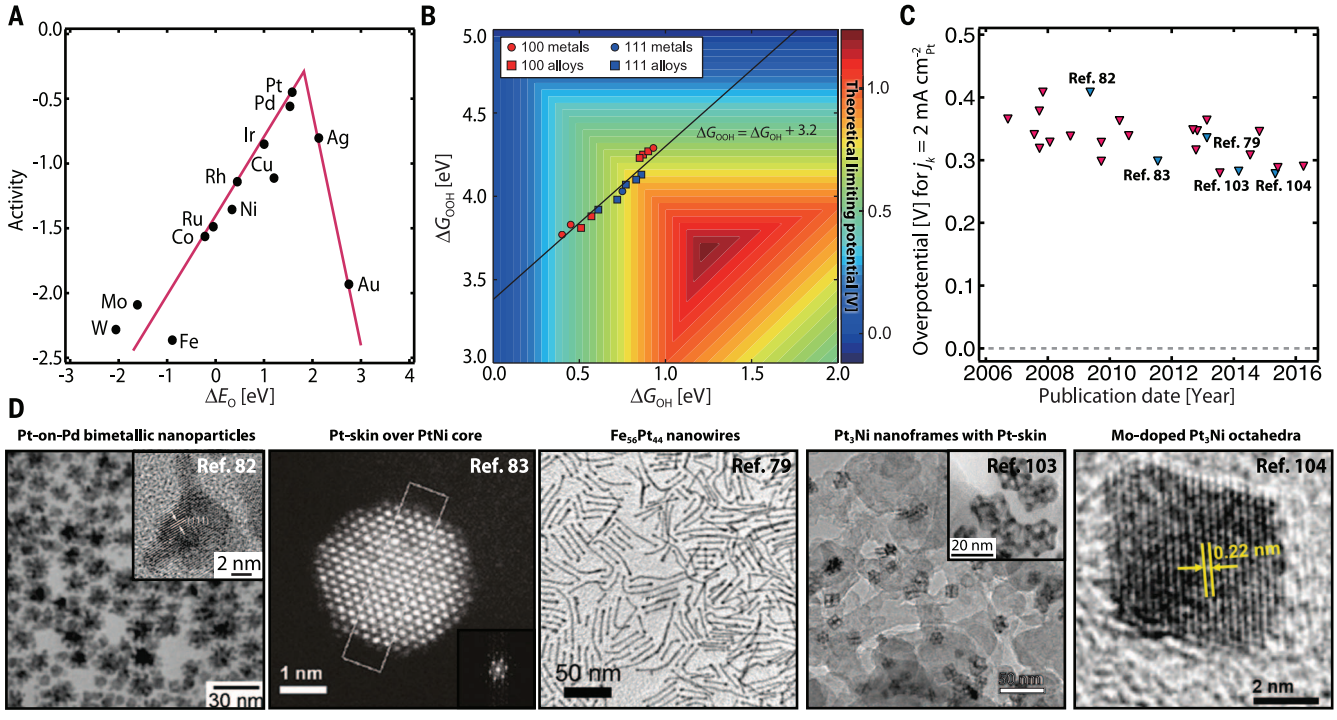

Fig. 4. The oxygen reduction reaction. (**A**) ORR volcano plot for metals. [Reproduced with permission from (*71*)] (**B**) ORR theoretical limiting potential plot for fcc (111) and (100) facets of metals and alloys. [Reproduced with permission from (*73*)] (**C**) Chronological trend in overpotential of Pt-based ORR catalysts. Data obtained from (*74*, *82*–*92*, *98*, *104*) and references therein. (**D**) Representative microscopy images of ORR catalysts. [Reproduced with permission from (*79*, *82*, *83*, *103*, *104*)]

undergo oxidation, which presents a different type of surface than that pertaining under ORR conditions (*107*, *108*). Again, an important frontier in catalysis research is the development of improved methods, both experimental and theoretical, that can rapidly and accurately ascertain the surface structure and stoichiometry of the catalyst material during different operating conditions. Such information is essential to gain a full understanding of the reaction kinetics and would put the community in a position to develop the best possible catalyst materials.

Because catalyst materials for the OER are generally metal oxides, volcano plots for the OER have been constructed for a wide variety of metal oxide surfaces (including rutile, perovskite, spinel, rock salt, and bixbyite oxides) using $\Delta G_O - \Delta G_{OH}$ as the descriptor (*109*). Experimental overpotentials at 1 mA cm^{-2}_{cat} are seen to overlay well on the theoretical overpotential volcano when plotted against this simple descriptor (Fig. 5A). A more complete model would incorporate, among other things, more precise depictions of the catalytically active surfaces involved; for instance, it has been observed that some of the perovskites (of chemical formula ABO_3) in Fig. 5A undergo leaching of either A or B metal cations and surface amorphization under OER conditions (*110*–*112*). In the absence of fully elucidated surface structures for the resulting catalytically active surfaces, binding energies from the ideal, stoichiometric terminations were used in the construction of Fig. 5A. All surfaces studied among these broad classes of metal oxide materials were found to obey a scaling relation between OOH* and OH* that is not ideal ($\Delta G_{OOH} = \Delta G_{OH} + 3.2 \pm 0.2$ eV), similar to the case of metals investigated for the ORR, again hindering the development of a catalyst with zero theoretical overpotential (*109*). For OER catalysis in acid, IrO_2 is a reasonably active metal oxide catalyst, as has been theoretically explained on the basis of reasonable binding energies to reaction intermediates (*113*–*117*). Although this catalyst has indeed been shown experimentally to be among the better OER catalysts today, based on activity and stability under reaction conditions, it is far from an ideal OER catalyst in terms of activity and is not completely stable under high oxidative potentials (*65*, *105*, *118*). Recently, thin films of IrO_x/$SrIrO_3$ were reported to show extremely high OER activity in acid (270 mV at 10 mA cm^{-2}_{oxide}, normalized to oxide surface area) along with promising stability (*119*). The associated geometric area–normalized activity is also exceptional (Fig. 5B) despite the low surface area of the films; leveraging the excellent intrinsic activity with formulations that provide higher surface area (Fig. 2) could lead to further improvements in overall electrode activity.

Owing to the high cost and scarcity of precious metals such as Pt, Ru, and Ir, non–precious metal oxide catalysts such as nickel oxides (*120*–*124*), cobalt oxides (*125*, *126*), manganese oxides (*127*), and multication perovskites (*128*–*130*) have also been vigorously studied, although they are stable only under alkaline conditions. Recently, electrodes of ternary FeCoW oxyhydroxides with high surface area were prepared (Fig. 5B), exhibiting low overpotential (191 mV at 10 mA cm^{-2}_{geo}) for the OER in alkaline electrolyte (*131*). When normalized to the catalyst surface area, many non–precious metal oxide catalysts for the OER are at least as active as precious metal–based systems in alkali (*65*, *118*). Some of these catalysts show bifunctional activity for both the ORR and OER in alkaline media as well. By studying a series of perovskites, a volcano-type relationship was established between ORR/OER activity and the filling of e_g orbitals in the surface metal cations, which can serve as another descriptor of activity (*128*, *129*). Optimal activity was found in the case of e_g occupancy close to unity, with high covalency of the transition metal–oxygen bond.

Metal-free catalysts have also recently emerged as a promising class of ORR/OER catalysts under alkaline conditions (e.g., heteroatom-doped carbons) (*132*–*134*). By doping carbon with more electronegative atoms such as nitrogen, a net positive charge is created on adjacent carbon atoms (C^+), which facilitates oxygen adsorption and charge transfer, resulting in enhanced ORR/OER activity (*132*). This strategy has also been extended to dopant atoms that are less electronegative than carbon (such as boron), which create similar charge sites (such as B^+) to facilitate the catalytic process (*133*). To exploit synergistic effects of different dopant atoms, co-doping of carbon catalysts has been demonstrated with success as well (*134*).

A typical shortcoming of non–precious metal oxide and metal-free catalysts, however, is their poor stability in an acidic environment (*65*, *118*). Overall, the development of Earth-abundant ORR/OER catalysts that possess both high activity and stability in acidic media (e.g., for proton exchange membrane fuel cells and electrolyzers) remains a serious challenge (*135*). To achieve progress in this direction, a deeper understanding of the working state of these catalysts and the nature of their active sites is needed so as to control and tailor their properties in the appropriate manner. A combination of theory, computational studies, and sophisticated in situ/in operando characterization techniques will help to address these critical issues.

Although the thermodynamic limiting potential volcanoes as in Fig. 4A have been helpful in elucidating trends in ORR/OER catalysis, it is desirable to move toward volcanoes derived from microkinetic modeling. In addition to the reaction energies of the elementary steps used in constructing the thermodynamic volcano, such a model requires information about the size of kinetic barriers for each elementary step. Whereas the calculation of kinetic barriers for non-electrochemical steps is well understood, the calculation of electrochemical kinetic barriers (including their potential dependence) is much more difficult with current techniques (*20*, *23*–*28*). In large part, this difficulty arises from the inherent restriction of DFT to calculations at constant charge rather than constant potential, which results in a changing potential across the reaction coordinate. One scheme to circumvent this limitation involves extrapolation to the limit of an infinite unit cell, where a single charge transfer has negligible impact on the simulated potential and thus the reaction energy and barrier are obtainable at constant potential. By performing calculations

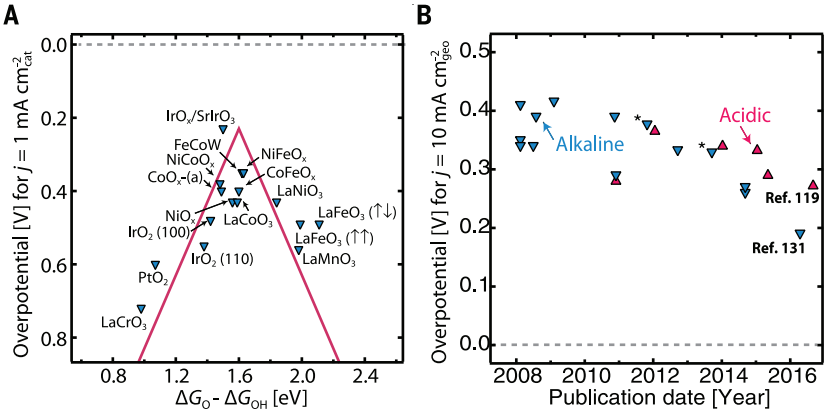

Fig. 5. The oxygen evolution reaction. (**A**) OER volcano plot for metal oxides. Experimental and theoretical data were respectively obtained from (*118*) and (*126*) for CoO_x-(a), $NiCoO_x$, and $CoFeO_x$; (*118*) and (*123*) for NiO_x and $NiFeO_x$; (*129*) and (*130*) for $LaMO_3$ perovskites (applied +0.21 eV reverse solvation correction to $\Delta G_O - \Delta G_{OH}$ for consistency with other data); (*113*) and (*117*) for IrO_2(110); (*113*) and (*119*) for IrO_2(100); (*107*) and (*109*) for PtO_2 [calculation assumes beta-($CaCl_2$) phase, which is more stable than the rutile phase according to (*108*)]; (*119*) for IrO_x/$SrIrO_3$ (calculation assumes IrO_3/$SrIrO_3$ active site); and (*131*) for FeCoW (calculation assumes FeW-doped CoOOH as active site). Current densities (extrapolated at constant Tafel slope where necessary) were normalized to surface area by capacitance in (*118*) and by Brunauer-Emmett-Teller measurements and scanning electron microscopy in (*129*, *131*). IrO_2 and IrO_x/$SrIrO_3$ films were found to be flat by atomic force microscopy. PtO_2 (10^{-9} mol cm^{-2} loading) was assumed to be flat. The volcano itself corresponds to $\Delta G_{OOH} = \Delta G_{OH} + 3.2$ eV (*109*). (**B**) Chronological trend in overpotential of various OER catalysts in acid and alkali. Data obtained from (*65*, *105*, *114*–*116*, *118*, *119*, *122*, *131*) and references therein. Data points marked with asterisks are normalized to oxide surface area.

with progressively larger unit cells, it has been possible to extrapolate to the infinite cell size limit, where a kinetic barrier of 0.26 eV was found at zero driving force and a charge transfer coefficient of 0.5 for the reduction of OH* to H_2O on Pt(111) (*25*).

Further studies have incorporated these kinetic parameters for all four coupled proton-electron transfer steps of the ORR into a steady-state microkinetic model to study Pt(111) (*136*). Additionally, the reaction energies and barriers used in the model were calculated in the presence of an explicit solvation bilayer of water and at the most stable coverage that has been found both experimentally and theoretically: a honeycomb $(\sqrt{3} \times \sqrt{3})R30$ pattern with 2/3 monolayer H_2O and 1/3 monolayer OH (*137*–*140*). The formation of the two-electron product H_2O_2 was also considered, as shown in the free energy diagram (Fig. 6A). Figure 6B compares the experimental (black/gray) and simulated (pink/blue) polarization curves (*141*, *142*). With the additional consideration of diffusion steps (pink), remarkable agreement is achieved between experiment and theory for both onset potential and saturation current density. Finally, the scaling relationships were used to generalize the model over a binding energy descriptor space and thus create a theoretical volcano derived from microkinetic modeling (Fig. 6C). This study demonstrates progress in the modeling of multistep electrochemical reactions at the complicated electrode-electrolyte interface, but the path forward requires even more detailed and efficient methods of determining electrochemical barriers, an important frontier ahead.

Despite extensive research over the years to develop ORR/OER catalysts in both acids and bases, most state-of-the-art catalysts still require far-from-ideal overpotentials of 0.25 to 0.4 V to reach current densities of interest (Figs. 4C and 5B) (*74*, *105*). The theoretical framework presented above shows that this is largely due to scaling relations among reactive intermediates involved in the ORR/OER. Overcoming this particular limitation requires decoupling the binding energies of different intermediates—for instance, by stabilizing OOH* with respect to OH* (*109*, *143*). Although the volcano framework has helped to elucidate this key concept, its implementation will require substantial effort. A deeper understanding of the electrode-electrolyte interface and the associated kinetics would allow for more detailed strategies to design ORR/OER catalysts with truly low overpotential. Developing a means to engineer a catalyst material around known scaling relations is just the first step in opening up opportunities to create near-ideal ORR/OER catalyst systems that would substantially increase the efficiency of a wide range of energy conversion devices.

Emerging reactions of interest

Beyond the aforementioned reactions involving the HER, HOR, ORR, and OER, there are a multitude of other emerging energy conversion reactions that are relatively less explored. Several of them could potentially be game-changing if electrocatalysts with the right properties could be developed. Although these reactions may involve a different set of reaction intermediates, mechanisms, and number of electrons transferred, the concepts of descriptors and volcanoes to assess activity and selectivity also represent a first important step in gaining the understanding needed to accelerate catalyst development in these areas.

Hydrogen peroxide production

The development of an electrochemical process to directly reduce oxygen to hydrogen peroxide ($O_2 + 2H^+ + 2e^- \rightarrow H_2O_2$) would be advantageous because it could replace the conventional, energy-intensive anthraquinone process with a protocol directly coupled to renewable electricity for safer deployment in a modular, decentralized fashion (*7*, *13*). The electrochemical reduction of oxygen to hydrogen peroxide has generally been explored in acidic environments because hydrogen peroxide decomposes under alkaline conditions (*7*, *13*).

Overall, the production of hydrogen peroxide from oxygen involves two coupled electron-proton transfers and one reaction intermediate (OOH*), making it similar in complexity to the HER (*13*):

$$O_2 + * + H^+ + e^- \rightarrow OOH* \quad (12)$$

$$OOH* + H^+ + e^- \rightarrow H_2O_2 + * \quad (13)$$

As such, it is possible to find a catalyst with zero theoretical overpotential that has an optimal ΔG_{OOH}, binding OOH* neither too strongly nor weakly (*13*). Although several catalysts, such as Pt (*144*), Ag (*145*), Au (*146*), Au-Pd alloys (*146*), nitrogen-doped carbon (*147*), and hierarchically porous carbon (*148*), have been explored, they were found to exhibit only modest performance in the production of hydrogen peroxide. Suitable electrocatalysts would need to possess high selectivity toward the two-electron as opposed to the four-electron pathway.

DFT calculations have established a volcano framework that relates the theoretical overpotential to ΔG_{OOH} for the two-electron reduction of oxygen to hydrogen peroxide (*13*), and experimental overpotentials at 1 mA cm^{-2} are overlaid on this plot (*149*) (Fig. 7A). For metals that bind OOH* strongly, the four-electron ORR will dominate over the two-electron pathway. On the other hand, in the case of weak OOH* binding, the two- and four-electron volcano plots overlap each other, which indicates a compromise in activity for hydrogen peroxide selectivity with weaker OOH* binding (*13*, *149*). As a result, the most promising catalyst with both high activity and selectivity toward hydrogen peroxide would be found at the apex of the two-electron volcano plot. Theoretically predicted Pt-Hg, Pd-Hg, and Ag-Hg alloys showed not only impressive mass activity but

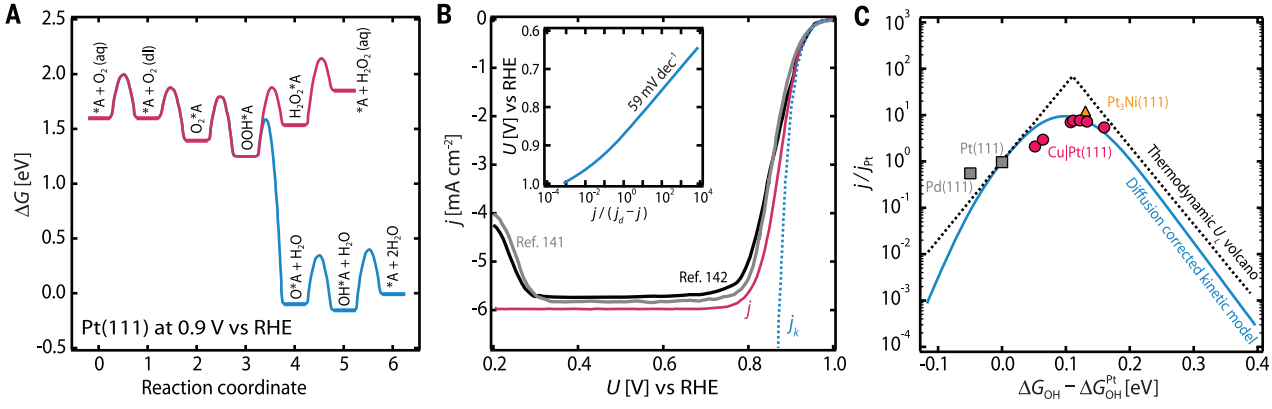

Fig. 6. Microkinetic modeling for the oxygen reduction reaction. (**A**) Free energy diagrams for O_2 reduction to H_2O and H_2O_2 on Pt(111) at 0.9 V versus RHE, showing the pathway for reduction to H_2O_2 and the dominating pathway to H_2O proceeding through electrochemical reduction of $OOH*_A$. [Reproduced with permission from (*136*)] (**B**) Simulated polarization curve and kinetic current density on Pt(111) at a rotation speed of 1600 rpm. Experimental polarization curves on Pt(111) at room temperature in 0.1 M $HClO_4$ at a rotation speed of 1600 rpm are shown for comparison (*141*, *142*). The inset shows a Tafel plot with a slope of 59 mV/decade indicated. [Reproduced with permission from (*136*)] (**C**) Simulated kinetic volcano at 0.9 V versus RHE compared to the limiting potential volcano and experiments on (111) facets, with experimental labels for Cu/Pt(111), Pt(111), Pt_3Ni(111), and Pd(111). [Reproduced with permission from (*136*)]

also high selectivity (>95%) in the synthesis of hydrogen peroxide (*13*, *149*). The rational design approach in this work has uncovered important concepts to begin screening and identifying more attractive catalyst candidates for this reaction, in particular to bypass the toxicity of Hg. Building on the thermodynamic-based framework and extending it to understand kinetic barriers and interfacial processes in greater detail, across a broader range of materials and reaction conditions, would help to provide further insights for the development of scalable catalysts that are selective to hydrogen peroxide while operating at low overpotentials.

Carbon dioxide reduction reaction

Another important energy conversion reaction involves the electroreduction of carbon dioxide to value-added products using renewable energy as an input (*14*). Like the ORR, this is a multielectron reduction reaction involving a number of different surface-bound reaction intermediates (*150*–*153*). However, unlike the ORR (which has only two major end products, water or hydrogen peroxide), there are a vast number of possible carbon dioxide reduction products, including carbon monoxide, formate, formaldehyde, methane, methanol, and C_{2+} hydrocarbons and oxygenates; many of these products require a large number of protons and electrons transferred, and possibly proceed through different intermediates as well (*150*–*153*). Thus, steering catalyst selectivity among the many carbon-based products is a major challenge, compounded by the fact that the equilibrium potentials for most of the carbon dioxide reduction half-reactions are close to 0 V versus RHE, making the HER an additional competing reaction beyond those toward unwanted carbon-based by-products (*150*–*153*). Therefore, for carbon dioxide reduction to be commercially viable, electrocatalysts would need to possess both high activity and high selectivity toward the particular product of interest.

In the 1980s, carbon dioxide reduction was investigated on a wide variety of heterogeneous elemental surfaces (*150*). The catalysts studied were broadly classified according to their selectivity toward their major product of reaction: (i) carbon monoxide (e.g., Au, Ag), (ii) formate (e.g., Pb, Sn), (iii) hydrocarbons (e.g., Cu), and (iv) hydrogen (e.g., Pt, Ni). On the basis of the combined theoretical and experimental framework described above, an initial volcano plot was constructed to understand catalytic trends in carbon dioxide reduction. Figure 7B consists of DFT calculations that relate the theoretical limiting potential to DFT-calculated ΔE_{CO} (*154*), and overlaid are experimental onset potentials for the formation of methane and/or methanol, the earliest potentials at which either product is detected (*155*). In the case of metals that bind CO* too strongly, the overpotential is dictated by the protonation of CO* to CHO*, whereas for metals that bind CO* too weakly, the overpotential is dictated by the protonation of $CO_{(g)}$ to CHO*, where CO desorption is the competing reaction (*154*). For the formation of methane/methanol, Cu was found to reside near the top of the volcano plot with optimal ΔE_{CO}, albeit with a substantial theoretical overpotential of ~0.8 V due to limitations from scaling relations (*154*, *155*). This is unsurprising, given the many reaction steps and intermediates involved for each product; several of the intermediates are C_1 species that likely bind to the metal in a similar manner (e.g., between the carbon atom and the metal surface) (*156*). Again, this points to the imperative of breaking the scaling relations among the various reaction intermediates—a necessary although perhaps insufficient condition for a carbon dioxide reduction catalyst that produces methane/methanol with increased activity by many orders of magnitude. Theoretical guidance suggests that strengthening the binding energy of CHO* (or, more precisely, the transition state energy for the coupled proton-electron transfer to adsorbed CO) relative to that of CO* would enable the protonation of CO* to CHO* at a less negative potential and lead to substantially lower overpotential (*153*). This can potentially be achieved through a number of strategies, including alloying, electrolyte additives, ionic liquids, tethering surface species, promoters, and hydrogen bond donors or acceptors (*153*, *157*).

The formation of C_{2+} species is yet more complex, as C-C bond formation is another reaction step to consider. Two pathways have been identified. In one pathway, carbon monoxide is first hydrogenated, which makes the formation of the C-C bond more facile (*158*). In the other pathway, adsorbed carbon monoxide dimerizes first (*159*–*161*). For ethanol formation, acetaldehyde was recently identified as an important intermediate (*162*). Given the complexity of the carbon dioxide reduction reaction, more computational and experimental work is needed to elucidate the underlying reaction mechanisms and intermediates. Further insight can also be gained by studying the related carbon monoxide reduction reaction, which is similar to carbon dioxide reduction but avoids potential catalyst-poisoning effects from the formation of formate (*161*–*163*).

Nitrogen reduction reaction

Inspiration for the electroreduction of nitrogen ($N_2 + 6H^+ + 6e^- \rightarrow 2NH_3$) can be drawn from the nitrogenase enzymes in bacteria that perform nitrogen fixation at room temperature and atmospheric pressure (*15*). Early studies demonstrated the feasibility of this process in a synthetic context (*164*, *165*), helping to motivate the development of catalysts including Pt (*166*), Rh (*167*), and Ru (*167*, *168*). As with carbon dioxide reduction, the nitrogen reduction reaction involves multiple intermediates, and the HER is a major competing reaction, making selectivity a great challenge (*15*). Experimental results so far show extremely poor performance (high overpotentials, low current densities, and low selectivity); there is much room for improvement (*15*).

To provide theoretical guidance, a volcano plot was constructed using DFT calculations to relate the theoretical limiting potential to ΔE_N on a variety of metal surfaces (Fig. 7C) (*169*, *170*). This framework again provides a means to understand some of the key points to consider involving elemental metal catalysts for this reaction: Metals that bind nitrogen too weakly are

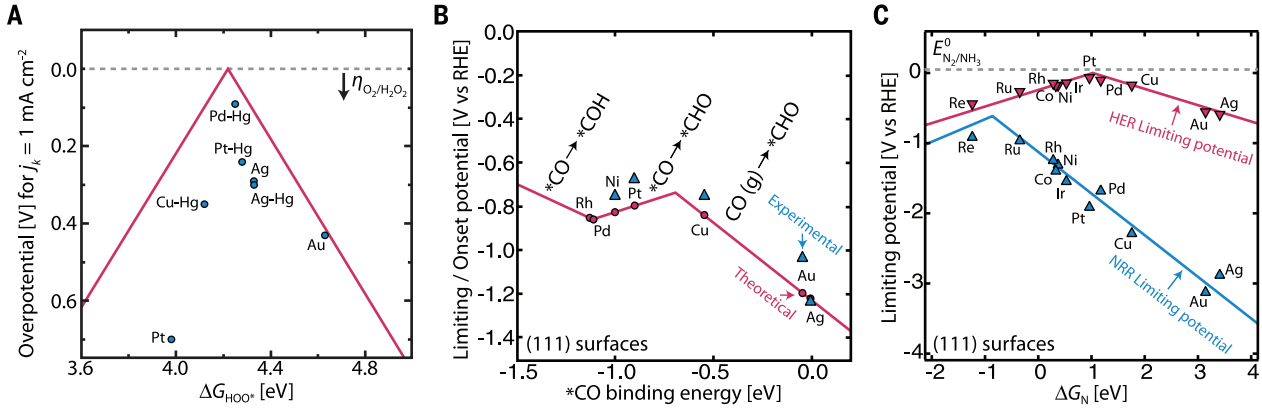

Fig. 7. Emerging reactions of interest. (**A**) Volcano plot for hydrogen peroxide production on metals and alloys. [Reproduced with permission from (*149*)] (**B**) Volcano plot for carbon dioxide reduction on metals. [Reproduced with permission from (*154*, *155*)] (**C**) Volcano plot for nitrogen reduction (NRR) on metals, with that of HER overlaid for comparison. [Reproduced with permission from (*170*)]

limited by the adsorption of N_2 as N_2H^* in the first step of the reaction, whereas strong-binding metals are limited by either the protonation of NH* to form NH_2^* (flat surfaces) or the removal of NH_2^* as NH_3 (stepped surfaces). Metals such as Ru, Rh, Mo, and Fe were calculated to lie near the top of the volcano plot, binding nitrogen neither too strongly nor too weakly (*169*). Unfortunately, even those metals that are found near the top of the volcano exhibit large theoretical overpotentials of at least 0.5 V because of nonideal scaling relations between the intermediates. Modeling to this point suggests that a necessary, although perhaps not sufficient, condition for improved nitrogen reduction activity may be achieved by stabilizing N_2H^* relative to NH_2^* or NH* (*170*).

For catalysts near the top of the volcano, the HER was also found to be a competing reaction, both theoretically and experimentally, thus compromising the faradaic efficiency for nitrogen reduction (Fig. 7C) (*167*–*170*). It was proposed that flat surfaces of Re, Sc, Y, Ti, and Zr are capable of performing nitrogen reduction at –1 to –1.5 V versus RHE with substantial suppression of the HER attributable to their stronger binding of nitrogen relative to hydrogen, but the conclusion was that mechanisms to suppress HER are needed to obtain reasonable performance (*169*). In general, the difference between the theoretical limiting potential volcanoes for nitrogen reduction and for the HER is smallest for flat, strong binding surfaces (*170*). Further DFT studies also suggested transition metal nitrides, such as VN and ZrN, to be highly active for nitrogen reduction at low onset potentials while suppressing the HER (*171*). The materials design strategies emerging from initial theoretical insights represent a first and important step toward developing improved catalysts. Further work is needed to elucidate atomic-scale processes at the electrode-electrolyte interface, including the roles of solvents, cations, and anions as well as the kinetics of proton-electron transfer and N-N scission. A greater understanding of the mechanistic details at the interface would provide the guidance needed to implement more targeted strategies for the development of advanced electrocatalysts for this promising, yet largely underexplored, reaction (*172*).

Outlook

Recent years have witnessed a blossoming interest in the development of advanced electrocatalysts for clean energy conversion. We have highlighted the utility of an initial approach that examines the elementary steps of each reaction to identify the key intermediates involved, their bonding to surfaces, and the energetics of each step. For each reaction, we illustrated how this approach has helped to clarify key limitations among known catalysts systems and how that knowledge has led to successful strategies to develop improved electrocatalysts. In most of the reactions, the limited success so far with the catalysts known to date can be traced back to the limitations set by scaling relations that exist between energies of different adsorbed intermediates. One of the main conclusions is that a new paradigm for catalyst design is needed to circumvent these constraints (*73*), specifically focused on tuning the stabilization of one intermediate relative to another.

One strategy would be to construct three-dimensional catalytically active sites that bind different reaction intermediates (and transition states) in different ways. Examples could include alloying, doping (*173*, *174*), or the introduction of defects. Alternatively, scaling might be circumvented by selectively stabilizing the intermediates through some external mechanism. For instance, differences in size could be distinguished through catalyst structures that bind larger intermediates through multiple sites [e.g., confinement (*143*)]; differences in chemical functionalization (e.g., hydrogen bonds) or physical properties (e.g., dipole strength) could be exploited through the addition of molecules to the electrolyte or promoters/ligands to the surface (*153*), as illustrated in Fig. 2.

Further efforts are also needed to elucidate many details of the electrode-electrolyte interface that remain poorly understood to date. Current challenges include atomistic- and molecular-level depictions of the solvent, cations, and anions near the interface, as well as the kinetics and reaction barriers of key elementary steps involving proton/electron transfers, all under relevant reaction conditions. Therein lies the frontier of electrocatalysis research; with faster, more efficient methods to capture this understanding with more advanced methods both in theory and in experiment, additional information will come to light that can further guide the community toward catalysts that can operate with near-ideal efficiency and selectivity.

REFERENCES AND NOTES

1. J. A. Turner, Sustainable hydrogen production. *Science* **305**, 972–974 (2004). doi: 10.1126/science.1103197; pmid: 15310892
2. S. Chu, A. Majumdar, Opportunities and challenges for a sustainable energy future. *Nature* **488**, 294–303 (2012). doi: 10.1038/nature11475; pmid: 22895334
3. N. S. Lewis, D. G. Nocera, Powering the planet: Chemical challenges in solar energy utilization. *Proc. Natl. Acad. Sci. U.S.A.* **103**, 15729–15735 (2006). doi: 10.1073/pnas.0603395103; pmid: 17043226
4. "World Energy Outlook 2015" (International Energy Agency, 2015).
5. "The Outlook for Energy: A View to 2040" (Exxon Mobil Corporation, 2015).
6. G. A. Olah, A. Goeppert, G. K. S. Prakash, *Beyond Oil and Gas: The Methanol Economy* (Wiley-VCH, 2009).
7. J. M. Campos-Martin, G. Blanco-Brieva, J. L. G. Fierro, Hydrogen peroxide synthesis: An outlook beyond the anthraquinone process. *Angew. Chem. Int. Ed.* **45**, 6962–6984 (2006). doi: 10.1002/anie.200503779; pmid: 17039551
8. "Mineral Commodity Summaries" (U.S. Geological Survey, 2015).
9. Y. Jiao, Y. Zheng, M. Jaroniec, S. Z. Qiao, Design of electrocatalysts for oxygen- and hydrogen-involving energy conversion reactions. *Chem. Soc. Rev.* **44**, 2060–2086 (2015). doi: 10.1039/C4CS00470A; pmid: 25672249
10. J. D. Benck, T. R. Hellstern, J. Kibsgaard, P. Chakthranont, T. F. Jaramillo, Catalyzing the hydrogen evolution reaction (HER) with molybdenum sulfide nanomaterials. *ACS Catal.* **4**, 3957–3971 (2014). doi: 10.1021/cs500923c
11. H. A. Gasteiger, S. S. Kocha, B. Sompalli, F. T. Wagner, Activity benchmarks and requirements for Pt, Pt-alloy, and non-Pt oxygen reduction catalysts for PEMFCs. *Appl. Catal. B* **56**, 9–35 (2005). doi: 10.1016/j.apcatb.2004.06.021
12. H. A. Gasteiger, N. M. Marković, Just a dream—or future reality? *Science* **324**, 48–49 (2009). doi: 10.1126/science.1172083; pmid: 19342578
13. S. Siahrostami *et al.*, Enabling direct H_2O_2 production through rational electrocatalyst design. *Nat. Mater.* **12**, 1137–1143 (2013). doi: 10.1038/nmat3795; pmid: 24240242
14. D. T. Whipple, P. J. A. Kenis, Prospects of CO_2 utilization via direct heterogeneous electrochemical reduction. *J. Phys. Chem. Lett.* **1**, 3451–3458 (2010). doi: 10.1021/jz1012627
15. C. J. M. van der Ham, M. T. M. Koper, D. G. H. Hetterscheid, Challenges in reduction of dinitrogen by proton and electron transfer. *Chem. Soc. Rev.* **43**, 5183–5191 (2014). doi: 10.1039/C4CS00085D; pmid: 24802308
16. R. Parsons, The rate of electrolytic hydrogen evolution and the heat of adsorption of hydrogen. *Trans. Faraday Soc.* **54**, 1053–1063 (1958). doi: 10.1039/tf9585401053
17. J. K. Nørskov *et al.*, Trends in the exchange current for hydrogen evolution. *J. Electrochem. Soc.* **152**, J23–J26 (2005). doi: 10.1149/1.1856988
18. J. Greeley, M. Mavrikakis, Alloy catalysts designed from first principles. *Nat. Mater.* **3**, 810–815 (2004). doi: 10.1038/nmat1223; pmid: 15502837
19. J. Greeley, T. F. Jaramillo, J. Bonde, I. B. Chorkendorff, J. K. Nørskov, Computational high-throughput screening of electrocatalytic materials for hydrogen evolution. *Nat. Mater.* **5**, 909–913 (2006). doi: 10.1038/nmat1752; pmid: 17041585
20. E. Skúlason *et al.*, Modeling the electrochemical hydrogen oxidation and evolution reactions on the basis of density functional theory calculations. *J. Phys. Chem. C* **114**, 18182–18197 (2010). doi: 10.1021/jp1048887
21. D. Strmcnik *et al.*, Improving the hydrogen oxidation reaction rate by promotion of hydroxyl adsorption. *Nat. Chem.* **5**, 300–306 (2013). doi: 10.1038/nchem.1574; pmid: 23511418
22. N. Danilovic, R. Subbaraman, D. Strmcnik, V. R. Stamenkovic, N. M. Markovic, Electrocatalysis of the HER in acid and alkaline media. *J. Serb. Chem. Soc.* **78**, 2007–2015 (2013). doi: 10.2298/JSC131118136D
23. Y. Huang, R. J. Nielsen, W. A. Goddard 3rd, M. P. Soriaga, The reaction mechanism with free energy barriers for electrochemical dihydrogen evolution on MoS_2. *J. Am. Chem. Soc.* **137**, 6692–6698 (2015). doi: 10.1021/jacs.5b03329; pmid: 25941943
24. Y.-H. Fang, Z.-P. Liu, Surface phase diagram and oxygen coupling kinetics on flat and stepped Pt surfaces under electrochemical potentials. *J. Phys. Chem. C* **113**, 9765–9772 (2009). doi: 10.1021/jp901091a
25. V. Tripković, E. Skúlason, S. Siahrostami, J. K. Nørskov, J. Rossmeisl, The oxygen reduction reaction mechanism on Pt(111) from density functional theory calculations. *Electrochim. Acta* **55**, 7975–7981 (2010). doi: 10.1016/j.electacta.2010.02.056
26. Y.-H. Fang, Z.-P. Liu, Mechanism and Tafel lines of electro-oxidation of water to oxygen on RuO_2(110). *J. Am. Chem. Soc.* **132**, 18214–18222 (2010). doi: 10.1021/ja1069272; pmid: 21133410
27. K. Chan, J. K. Nørskov, Electrochemical barriers made simple. *J. Phys. Chem. Lett.* **6**, 2663–2668 (2015). doi: 10.1021/acs.jpclett.5b01043; pmid: 26266844
28. K. Chan, J. K. Nørskov, Potential dependence of electrochemical barriers from ab initio calculations. *J. Phys. Chem. Lett.* **7**, 1686–1690 (2016). doi: 10.1021/acs.jpclett.6b00382; pmid: 27088442
29. H. Tributsch, J. C. Bennett, Electrochemistry and photochemistry of MoS_2 layer crystals. 1. *J. Electroanal. Chem.* **81**, 97–111 (1977). doi: 10.1016/S0022-0728(77)80363-X
30. B. Hinnemann *et al.*, Biomimetic hydrogen evolution: MoS_2 nanoparticles as catalyst for hydrogen evolution. *J. Am. Chem. Soc.* **127**, 5308–5309 (2005). doi: 10.1021/ja0504690; pmid: 15826154
31. C. Tsai, K. R. Chan, J. K. Nørskov, F. Abild-Pedersen, Theoretical insights into the hydrogen evolution activity of layered transition metal dichalcogenides. *Surf. Sci.* **640**, 133–140 (2015). doi: 10.1016/j.susc.2015.01.019
32. T. F. Jaramillo *et al.*, Identification of active edge sites for electrochemical H_2 evolution from MoS_2 nanocatalysts. *Science* **317**, 100–102 (2007). doi: 10.1126/science.1141483; pmid: 17615351
33. J. Kibsgaard, Z. Chen, B. N. Reinecke, T. F. Jaramillo, Engineering the surface structure of MoS_2 to preferentially expose active edge sites for electrocatalysis. *Nat. Mater.* **11**, 963–969 (2012). doi: 10.1038/nmat3439; pmid: 23042413

34. Z. Chen *et al*., Core-shell MoO_3-MoS_2 nanowires for hydrogen evolution: A functional design for electrocatalytic materials. *Nano Lett.* **11**, 4168–4175 (2011). doi: 10.1021/nl2020476; pmid: 21894935
35. D. Kong *et al*., Synthesis of MoS_2 and $MoSe_2$ films with vertically aligned layers. *Nano Lett.* **13**, 1341–1347 (2013). doi: 10.1021/nl400258t; pmid: 23387444
36. H. Wang *et al*., Electrochemical tuning of vertically aligned MoS_2 nanofilms and its application in improving hydrogen evolution reaction. *Proc. Natl. Acad. Sci. U.S.A.* **110**, 19701–19706 (2013). doi: 10.1073/pnas.1316792110; pmid: 24248362
37. Y. Li *et al*., MoS_2 nanoparticles grown on graphene: An advanced catalyst for the hydrogen evolution reaction. *J. Am. Chem. Soc.* **133**, 7296–7299 (2011). doi: 10.1021/ja201269b; pmid: 21510646
38. M. A. Lukowski *et al*., Enhanced hydrogen evolution catalysis from chemically exfoliated metallic MoS_2 nanosheets. *J. Am. Chem. Soc.* **135**, 10274–10277 (2013). doi: 10.1021/ja404523s; pmid: 23790049
39. D. Voiry *et al*., Conducting MoS_2 nanosheets as catalysts for hydrogen evolution reaction. *Nano Lett.* **13**, 6222–6227 (2013). doi: 10.1021/nl403661s; pmid: 24251828
40. D. Voiry *et al*., Enhanced catalytic activity in strained chemically exfoliated WS_2 nanosheets for hydrogen evolution. *Nat. Mater.* **12**, 850–855 (2013). doi: 10.1038/nmat3700; pmid: 23832127
41. H. Li *et al*., Activating and optimizing MoS_2 basal planes for hydrogen evolution through the formation of strained sulphur vacancies. *Nat. Mater.* **15**, 48–53 (2016). doi: 10.1038/nmat4465; pmid: 26552057
42. D. Merki, S. Fierro, H. Vrubel, X. L. Hu, Amorphous molybdenum sulfide films as catalysts for electrochemical hydrogen production in water. *Chem. Sci.* **2**, 1262–1267 (2011). doi: 10.1039/C1SC00117E
43. J. D. Benck, Z. B. Chen, L. Y. Kuritzky, A. J. Forman, T. F. Jaramillo, Amorphous molybdenum sulfide catalysts for electrochemical hydrogen production: Insights into the origin of their catalytic activity. *ACS Catal.* **2**, 1916–1923 (2012). doi: 10.1021/cs300451q
44. H. G. S. Casalongue *et al*., Operando characterization of an amorphous molybdenum sulfide nanoparticle catalyst during the hydrogen evolution reaction. *J. Phys. Chem. C* **118**, 29252–29259 (2014). doi: 10.1021/jp505394e
45. D. Merki, H. Vrubel, L. Rovelli, S. Fierro, X. L. Hu, Fe, Co, and Ni ions promote the catalytic activity of amorphous molybdenum sulfide films for hydrogen evolution. *Chem. Sci.* **3**, 2515–2525 (2012). doi: 10.1039/c2sc20539d
46. J. Kristensen, J. Zhang, I. Chorkendorff, J. Ulstrup, B. L. Ooi, Assembled monolayers of $Mo_3S_4^{4+}$ clusters on well-defined surfaces. *Dalton Trans.* **2006**, 3985–3990 (2006). doi: 10.1039/b608949f; pmid: 17028707
47. T. F. Jaramillo *et al*., Hydrogen evolution on supported incomplete cubane-type $[Mo_3S_4]^{4+}$ electrocatalysts. *J. Phys. Chem. C* **112**, 17492–17498 (2008). doi: 10.1021/jp802695e
48. H. I. Karunadasa *et al*., A molecular MoS_2 edge site mimic for catalytic hydrogen generation. *Science* **335**, 698–702 (2012). doi: 10.1126/science.1215868; pmid: 22323816
49. J. Kibsgaard, T. F. Jaramillo, F. Besenbacher, Building an appropriate active-site motif into a hydrogen-evolution catalyst with thiomolybdate $[Mo_3S_{13}]^{2-}$ clusters. *Nat. Chem.* **6**, 248–253 (2014). doi: 10.1038/nchem.1853; pmid: 24557141
50. E. J. Popczun, C. G. Read, C. W. Roske, N. S. Lewis, R. E. Schaak, Highly active electrocatalysis of the hydrogen evolution reaction by cobalt phosphide nanoparticles. *Angew. Chem. Int. Ed.* **53**, 5427–5430 (2014). doi: 10.1002/anie.201402646; pmid: 24729482
51. J. Kibsgaard, T. F. Jaramillo, Molybdenum phosphosulfide: An active, acid-stable, earth-abundant catalyst for the hydrogen evolution reaction. *Angew. Chem. Int. Ed.* **53**, 14433–14437 (2014). doi: 10.1002/anie.201408222; pmid: 25359678
52. A. B. Laursen *et al*., Nanocrystalline Ni_5P_4: A hydrogen evolution electrocatalyst of exceptional efficiency in both alkaline and acidic media. *Energy Environ. Sci.* **8**, 1027–1034 (2015). doi: 10.1039/C4EE02940B
53. Q. Liu *et al*., Carbon nanotubes decorated with CoP nanocrystals: A highly active non-noble-metal nanohybrid electrocatalyst for hydrogen evolution. *Angew. Chem. Int. Ed.* **53**, 6710–6714 (2014). doi: 10.1002/anie.201404161; pmid: 24845625
54. J. Tian, Q. Liu, A. M. Asiri, X. Sun, Self-supported nanoporous cobalt phosphide nanowire arrays: An efficient 3D hydrogen-evolving cathode over the wide range of pH 0-14. *J. Am. Chem. Soc.* **136**, 7587–7590 (2014). doi: 10.1021/ja503372r; pmid: 24830333
55. J. Hao, W. Yang, Z. Zhang, J. Tang, Metal-organic frameworks derived $Co_xFe_{1-x}P$ nanocubes for electrochemical hydrogen evolution. *Nanoscale* **7**, 11055–11062 (2015). doi: 10.1039/C5NR01955A; pmid: 26052656
56. E. J. Popczun *et al*., Nanostructured nickel phosphide as an electrocatalyst for the hydrogen evolution reaction. *J. Am. Chem. Soc.* **135**, 9267–9270 (2013). doi: 10.1021/ja403440e; pmid: 23763295
57. J. M. McEnaney *et al*., Amorphous molybdenum phosphide nanoparticles for electrocatalytic hydrogen evolution. *Chem. Mater.* **26**, 4826–4831 (2014). doi: 10.1021/cm502035s
58. J. F. Callejas *et al*., Electrocatalytic and photocatalytic hydrogen production from acidic and neutral-pH aqueous solutions using iron phosphide nanoparticles. *ACS Nano* **8**, 11101–11107 (2014). doi: 10.1021/nn5048553; pmid: 25250976
59. J. Kibsgaard *et al*., Designing an improved transition metal phosphide catalyst for hydrogen evolution using experimental and theoretical trends. *Energy Environ. Sci.* **8**, 3022–3029 (2015). doi: 10.1039/C5EE02179K
60. F. H. Saadi *et al*., Operand synthesis of macroporous molybdenum diselenide films for electrocatalysis of the hydrogen-evolution reaction. *ACS Catal.* **4**, 2866–2873 (2014). doi: 10.1021/cs500412u
61. H. Vrubel, X. Hu, Molybdenum boride and carbide catalyze hydrogen evolution in both acidic and basic solutions. *Angew. Chem. Int. Ed.* **51**, 12703–12706 (2012). doi: 10.1002/anie.201207111; pmid: 23143996
62. Z. W. Seh *et al*., Two-dimensional molybdenum carbide (MXene) as an efficient electrocatalyst for hydrogen evolution. *ACS Energy Lett.* **1**, 589–594 (2016). doi: 10.1021/acsenergylett.6b00247
63. W. F. Chen *et al*., Hydrogen-evolution catalysts based on non-noble metal nickel-molybdenum nitride nanosheets. *Angew. Chem. Int. Ed.* **51**, 6131–6135 (2012). doi: 10.1002/anie.201200699; pmid: 22565496
64. J. R. McKone, B. F. Sadtler, C. A. Werlang, N. S. Lewis, H. B. Gray, Ni-Mo nanopowders for efficient electrochemical hydrogen evolution. *ACS Catal.* **3**, 166–169 (2013). doi: 10.1021/cs300691m
65. C. C. L. McCrory *et al*., Benchmarking hydrogen evolving reaction and oxygen evolving reaction electrocatalysts for solar water splitting devices. *J. Am. Chem. Soc.* **137**, 4347–4357 (2015). doi: 10.1021/ja510442p; pmid: 25668483
66. T. R. Hellstern, J. D. Benck, J. Kibsgaard, C. Hahn, T. F. Jaramillo, Engineering cobalt phosphide (CoP) thin film catalysts for enhanced hydrogen evolution activity on silicon photocathodes. *Adv. Energy Mater.* **6**, 1501758 (2016). doi: 10.1002/aenm.201501758
67. W. A. Hoffert, J. A. S. Roberts, R. M. Bullock, M. L. Helm, Production of H_2 at fast rates using a nickel electrocatalyst in water-acetonitrile solutions. *Chem. Commun.* **49**, 7767–7769 (2013). doi: 10.1039/c3cc43203c; pmid: 23743801
68. J. Hou *et al*., Electrocatalytic H_2 production with a turnover frequency $>10^7$ s^{-1}: The medium provides an increase in rate but not overpotential. *Energy Environ. Sci.* **7**, 4013–4017 (2014). doi: 10.1039/C4EE01899K
69. H. J. S. Brown, S. Wiese, J. A. S. Roberts, R. M. Bullock, M. L. Helm, Electrocatalytic hydrogen production by $[Ni(7P^{Ph}{}_2N^{Et})_2]^{2+}$: Removing the distinction between endo- and exo-protonation sites. *ACS Catal.* **5**, 2116–2123 (2015). doi: 10.1021/cs502132y
70. W. C. Sheng, H. A. Gasteiger, Y. Shao-Horn, Hydrogen oxidation and evolution reaction kinetics on platinum: Acid vs alkaline electrolytes. *J. Electrochem. Soc.* **157**, B1529–B1536 (2010). doi: 10.1149/1.3483106
71. J. K. Nørskov *et al*., Origin of the overpotential for oxygen reduction at a fuel-cell cathode. *J. Phys. Chem. B* **108**, 17886–17892 (2004). doi: 10.1021/jp047349j
72. V. Viswanathan, H. A. Hansen, J. Rossmeisl, J. K. Nørskov, Universality in oxygen reduction electrocatalysis on metal surfaces. *ACS Catal.* **2**, 1654–1660 (2012). doi: 10.1021/cs300227s
73. A. Vojvodic, J. K. Nørskov, New design paradigm for heterogeneous catalysts. *Natl. Sci. Rev.* **2**, 140–149 (2015). doi: 10.1093/nsr/nwv023
74. C. M. Pedersen *et al*., Benchmarking Pt-based electrocatalysts for low temperature fuel cell reactions with the rotating disk electrode: Oxygen reduction and hydrogen oxidation in the presence of CO. *Electrochim. Acta* **179**, 647–657 (2015). doi: 10.1016/j.electacta.2015.03.176
75. N. M. Marković, R. R. Adzic, B. D. Cahan, E. B. Yeager, Structural effects in electrocatalysis—Oxygen reduction on platinum low-index single-crystal surfaces in perchloric-acid solutions. *J. Electroanal. Chem.* **377**, 249–259 (1994). doi: 10.1016/0022-0728(94)03467-2
76. M. E. Gamboa-Aldeco, E. Herrero, P. S. Zelenay, A. Wieckowski, Adsorption of bisulfate anion on a Pt(100) electrode—A comparison with Pt(111) and Pt(Poly). *J. Electroanal. Chem.* **348**, 451–457 (1993). doi: 10.1016/0022-0728(93)80151-7
77. C. Wang, H. Daimon, Y. Lee, J. Kim, S. Sun, Synthesis of monodisperse Pt nanocubes and their enhanced catalysis for oxygen reduction. *J. Am. Chem. Soc.* **129**, 6974–6975 (2007). doi: 10.1021/ja070440r; pmid: 17500520
78. Z. Chen, M. Waje, W. Li, Y. Yan, Supportless Pt and PtPd nanotubes as electrocatalysts for oxygen-reduction reactions. *Angew. Chem. Int. Ed.* **46**, 4060–4063 (2007). doi: 10.1002/anie.200700894; pmid: 17476642
79. S. Guo *et al*., FePt and CoPt nanowires as efficient catalysts for the oxygen reduction reaction. *Angew. Chem. Int. Ed.* **52**, 3465–3468 (2013). doi: 10.1002/anie.201209871; pmid: 23420804
80. B. Lim *et al*., Pd-Pt bimetallic nanodendrites with high activity for oxygen reduction. *Science* **324**, 1302–1305 (2009). doi: 10.1126/science.1170377; pmid: 19443738
81. L. Zhang *et al*., Platinum-based nanocages with subnanometer-thick walls and well-defined, controllable facets. *Science* **349**, 412–416 (2015). doi: 10.1126/science.aab0801; pmid: 26206931
82. Z. Peng, H. Yang, Synthesis and oxygen reduction electrocatalytic property of Pt-on-Pd bimetallic heteronanostructures. *J. Am. Chem. Soc.* **131**, 7542–7543 (2009). doi: 10.1021/ja902256a; pmid: 19438286
83. C. Wang *et al*., Design and synthesis of bimetallic electrocatalyst with multilayered Pt-skin surfaces. *J. Am. Chem. Soc.* **133**, 14396–14403 (2011). doi: 10.1021/ja2047655; pmid: 21770417
84. S. Chen *et al*., Enhanced activity for oxygen reduction reaction on "Pt_3Co" nanoparticles: Direct evidence of percolated and sandwich-segregation structures. *J. Am. Chem. Soc.* **130**, 13818–13819 (2008). doi: 10.1021/ja802513y; pmid: 18811156
85. M. H. Shao, K. Sasaki, P. Liu, R. R. Adzic, Pd_3Fe and Pt monolayer-modified Pd_3Fe electrocatalysts for oxygen reduction. *Z. Phys. Chem.* **221**, 1175–1190 (2007). doi: 10.1524/zpch.2007.221.9-10.1175
86. K. Sasaki, L. Zhang, R. R. Adzic, Niobium oxide-supported platinum ultra-low amount electrocatalysts for oxygen reduction. *Phys. Chem. Chem. Phys.* **10**, 159–167 (2008). doi: 10.1039/B709893F; pmid: 18075695
87. C. Cui, L. Gan, M. Heggen, S. Rudi, P. Strasser, Compositional segregation in shaped Pt alloy nanoparticles and their structural behaviour during electrocatalysis. *Nat. Mater.* **12**, 765–771 (2013). doi: 10.1038/nmat3668; pmid: 23770725
88. C. Cui *et al*., Octahedral PtNi nanoparticle catalysts: Exceptional oxygen reduction activity by tuning the alloy particle surface composition. *Nano Lett.* **12**, 5885–5889 (2012). doi: 10.1021/nl3032795; pmid: 23062102
89. P. Mani, R. Srivastava, P. Strasser, Dealloyed Pt-Cu core-shell nanoparticle electrocatalysts for use in PEM fuel cell cathodes. *J. Phys. Chem. C* **112**, 2770–2778 (2008). doi: 10.1021/jp0776412
90. S. Koh, M. F. Toney, P. Strasser, Activity-stability relationships of ordered and disordered alloy phases of Pt_3Co electrocatalysts for the oxygen reduction reaction (ORR). *Electrochim. Acta* **52**, 2765–2774 (2007). doi: 10.1016/j.electacta.2006.08.039
91. R. Srivastava, P. Mani, N. Hahn, P. Strasser, Efficient oxygen reduction fuel cell electrocatalysis on voltammetrically dealloyed Pt-Cu-Co nanoparticles. *Angew. Chem. Int. Ed.* **46**, 8988–8991 (2007). doi: 10.1002/anie.200703331; pmid: 17893897
92. D. Wang *et al*., Tuning oxygen reduction reaction activity via controllable dealloying: A model study of ordered Cu_3Pt/C intermetallic nanocatalysts. *Nano Lett.* **12**, 5230–5238 (2012). doi: 10.1021/nl302404g; pmid: 22954373
93. V. T. Ho, C.-J. Pan, J. Rick, W.-N. Su, B.-J. Hwang, Nanostructured $Ti_{0.7}Mo_{0.3}O_2$ support enhances electron transfer to Pt: High-performance catalyst for oxygen reduction reaction. *J. Am. Chem. Soc.* **133**, 11716–11724 (2011). doi: 10.1021/ja2039562; pmid: 21707063

94. Y. Liu, W. E. Mustain, High stability, high activity Pt/ITO oxygen reduction electrocatalysts. *J. Am. Chem. Soc.* **135**, 530–533 (2013). doi: 10.1021/ja307635r; pmid: 23270418
95. V. Stamenkovic *et al*., Changing the activity of electrocatalysts for oxygen reduction by tuning the surface electronic structure. *Angew. Chem. Int. Ed.* **45**, 2897–2901 (2006). doi: 10.1002/anie.200504386; pmid: 16596688
96. V. R. Stamenkovic *et al*., Trends in electrocatalysis on extended and nanoscale Pt-bimetallic alloy surfaces. *Nat. Mater.* **6**, 241–247 (2007). doi: 10.1038/nmat1840; pmid: 17310139
97. J. Greeley *et al*., Alloys of platinum and early transition metals as oxygen reduction electrocatalysts. *Nat. Chem.* **1**, 552–556 (2009). doi: 10.1038/nchem.367; pmid: 21378936
98. M. Escudero-Escribano *et al*., Tuning the activity of Pt alloy electrocatalysts by means of the lanthanide contraction. *Science* **352**, 73–76 (2016). doi: 10.1126/science.aad8892; pmid: 27034369
99. P. Hernandez-Fernandez *et al*., Mass-selected nanoparticles of PtxY as model catalysts for oxygen electroreduction. *Nat. Chem.* **6**, 732–738 (2014). pmid: 25054945
100. M. Escudero-Escribano *et al*., Pt_5Gd as a highly active and stable catalyst for oxygen electroreduction. *J. Am. Chem. Soc.* **134**, 16476–16479 (2012). doi: 10.1021/ja306348d; pmid: 22998588
101. A. Velázquez-Palenzuela *et al*., The enhanced activity of mass-selected Pt_xGd nanoparticles for oxygen electroreduction. *J. Catal.* **328**, 297–307 (2015). doi: 10.1016/j.jcat.2014.12.012
102. V. R. Stamenkovic *et al*., Improved oxygen reduction activity on $Pt_3Ni(111)$ via increased surface site availability. *Science* **315**, 493–497 (2007). doi: 10.1126/science.1135941; pmid: 17218494
103. C. Chen *et al*., Highly crystalline multimetallic nanoframes with three-dimensional electrocatalytic surfaces. *Science* **343**, 1339–1343 (2014). doi: 10.1126/science.1249061; pmid: 24578531
104. X. Huang *et al*., High-performance transition metal-doped Pt_3Ni octahedra for oxygen reduction reaction. *Science* **348**, 1230–1234 (2015). doi: 10.1126/science.aaa8765; pmid: 26068847
105. R. Frydendal *et al*., Benchmarking the stability of oxygen evolution reaction catalysts: The importance of monitoring mass losses. *Chemelectrochem* **1**, 2075–2081 (2014). doi: 10.1002/celc.201402262
106. J. Rossmeisl, Z. W. Qu, H. Zhu, G. J. Kroes, J. K. Nørskov, Electrolysis of water on oxide surfaces. *J. Electroanal. Chem.* **607**, 83–89 (2007). doi: 10.1016/j.jelechem.2006.11.008
107. C. Iwakura, K. Fukuda, H. Tamura, The anodic evolution of oxygen on platinum oxide electrode in alkaline solutions. *Electrochim. Acta* **21**, 501–508 (1976). doi: 10.1016/0013-4686(76)85139-0
108. S. Zhuo, K. Sohlberg, Platinum dioxide phases: Relative thermodynamic stability and kinetics of inter-conversion from first-principles. *Physica B* **381**, 12–19 (2006). doi: 10.1016/j.physb.2005.11.170
109. I. C. Man *et al*., Universality in oxygen evolution electrocatalysis on oxide surfaces. *ChemCatChem* **3**, 1159–1165 (2011). doi: 10.1002/cctc.201000397
110. K. J. May *et al*., Influence of oxygen evolution during water oxidation on the surface of perovskite oxide catalysts. *J. Phys. Chem. Lett.* **3**, 3264–3270 (2012). doi: 10.1021/jz301414z
111. M. Risch *et al*., Structural changes of cobalt-based perovskites upon water oxidation investigated by EXAFS. *J. Phys. Chem. C* **117**, 8628–8635 (2013). doi: 10.1021/jp3126768
112. B. Han *et al*., Activity and stability trends of perovskite oxides for oxygen evolution catalysis at neutral pH. *Phys. Chem. Chem. Phys.* **17**, 22576–22580 (2015). doi: 10.1039/C5CP04248H; pmid: 26271910
113. K. A. Stoerzinger, L. Qiao, M. D. Biegalski, Y. Shao-Horn, Orientation-dependent oxygen evolution activities of rutile IrO_2 and RuO_2. *J. Phys. Chem. Lett.* **5**, 1636–1641 (2014). doi: 10.1021/jz500610u; pmid: 26270358
114. Y. Lee, J. Suntivich, K. J. May, E. E. Perry, Y. Shao-Horn, Synthesis and activities of rutile IrO_2 and RuO_2 nanoparticles for oxygen evolution in acid and alkaline solutions. *J. Phys. Chem. Lett.* **3**, 399–404 (2012). doi: 10.1021/jz2016507; pmid: 26285858
115. M. Bernicke *et al*., Iridium oxide coatings with templated porosity as highly active oxygen evolution catalysts: Structure-activity relationships. *ChemSusChem* **8**, 1908–1915 (2015). doi: 10.1002/cssc.201402988; pmid: 25958795
116. H. N. Nong *et al*., Oxide-supported $IrNiO_x$ core-shell particles as efficient, cost-effective, and stable catalysts for electrochemical water splitting. *Angew. Chem. Int. Ed.* **54**, 2975–2979 (2015). doi: 10.1002/anie.201411072
117. M. García-Melchor, L. Vilella, N. López, A. Vojvodic, Computationally probing the performance of hybrid, heterogeneous, and homogeneous iridium-based catalysts for water oxidation. *ChemCatChem* **8**, 1792–1798 (2016). doi: 10.1002/cctc.201600007
118. C. C. L. McCrory, S. Jung, J. C. Peters, T. F. Jaramillo, Benchmarking heterogeneous electrocatalysts for the oxygen evolution reaction. *J. Am. Chem. Soc.* **135**, 16977–16987 (2013). doi: 10.1021/ja407115p; pmid: 24171402
119. L. C. Seitz *et al*., A highly active and stable $IrO_x/SrIrO_3$ catalyst for the oxygen evolution reaction. *Science* **353**, 1011–1014 (2016). doi: 10.1126/science.aaf5050; pmid: 27701108
120. J. Landon *et al*., Spectroscopic characterization of mixed Fe-Ni oxide electrocatalysts for the oxygen evolution reaction in alkaline electrolytes. *ACS Catal.* **2**, 1793–1801 (2012). doi: 10.1021/cs3002644
121. L. Trotochaud, J. K. Ranney, K. N. Williams, S. W. Boettcher, Solution-cast metal oxide thin film electrocatalysts for oxygen evolution. *J. Am. Chem. Soc.* **134**, 17253–17261 (2012). doi: 10.1021/ja307507a; pmid: 22991896
122. B. M. Hunter *et al*., Highly active mixed-metal nanosheet water oxidation catalysts made by pulsed-laser ablation in liquids. *J. Am. Chem. Soc.* **136**, 13118–13121 (2014). doi: 10.1021/ja506087h; pmid: 25197774
123. D. Friebel *et al*., Identification of highly active Fe sites in (Ni,Fe)OOH for electrocatalytic water splitting. *J. Am. Chem. Soc.* **137**, 1305–1313 (2015). doi: 10.1021/ja511559d; pmid: 25562406
124. J. W. D. Ng *et al*., Gold-supported cerium-doped NiO_x catalysts for water oxidation. *Nat. Energy* **1**, 16053 (2016). doi: 10.1038/nenergy.2016.53
125. Y. Liang *et al*., Co_3O_4 nanocrystals on graphene as a synergistic catalyst for oxygen reduction reaction. *Nat. Mater.* **10**, 780–786 (2011). doi: 10.1038/nmat3087; pmid: 21822263
126. M. Bajdich, M. García-Mota, A. Vojvodic, J. K. Nørskov, A. T. Bell, Theoretical investigation of the activity of cobalt oxides for the electrochemical oxidation of water. *J. Am. Chem. Soc.* **135**, 13521–13530 (2013). doi: 10.1021/ja405997s; pmid: 23944254
127. Y. Gorlin, T. F. Jaramillo, A bifunctional nonprecious metal catalyst for oxygen reduction and water oxidation. *J. Am. Chem. Soc.* **132**, 13612–13614 (2010). doi: 10.1021/ja104587v; pmid: 20839797
128. J. Suntivich *et al*., Design principles for oxygen-reduction activity on perovskite oxide catalysts for fuel cells and metal-air batteries. *Nat. Chem.* **3**, 546–550 (2011). doi: 10.1038/nchem.1069; pmid: 21697876
129. J. Suntivich, K. J. May, H. A. Gasteiger, J. B. Goodenough, Y. Shao-Horn, A perovskite oxide optimized for oxygen evolution catalysis from molecular orbital principles. *Science* **334**, 1383–1385 (2011). doi: 10.1126/science.1212858; pmid: 22033519
130. Y.-L. Lee, M. J. Gadre, Y. Shao-Horn, D. Morgan, Ab initio GGA+U study of oxygen evolution and oxygen reduction electrocatalysis on the (001) surfaces of lanthanum transition metal perovskites $LaBO_3$ (B = Cr, Mn, Fe, Co and Ni). *Phys. Chem. Chem. Phys.* **17**, 21643–21663 (2015). doi: 10.1039/C5CP02834E; pmid: 26227442
131. B. Zhang *et al*., Homogeneously dispersed multimetal oxygen-evolving catalysts. *Science* **352**, 333–337 (2016). doi: 10.1126/science.aaf1525; pmid: 27013427
132. K. Gong, F. Du, Z. Xia, M. Durstock, L. Dai, Nitrogen-doped carbon nanotube arrays with high electrocatalytic activity for oxygen reduction. *Science* **323**, 760–764 (2009). doi: 10.1126/science.1168049; pmid: 19197058
133. L. Yang *et al*., Boron-doped carbon nanotubes as metal-free electrocatalysts for the oxygen reduction reaction. *Angew. Chem. Int. Ed.* **50**, 7132–7135 (2011). doi: 10.1002/anie.201101287; pmid: 21688363
134. J. Zhang, Z. Zhao, Z. Xia, L. Dai, A metal-free bifunctional electrocatalyst for oxygen reduction and oxygen evolution reactions. *Nat. Nanotechnol.* **10**, 444–452 (2015). doi: 10.1038/nnano.2015.48; pmid: 25849787
135. R. Frydendal, E. A. Paoli, I. Chorkendorff, J. Rossmeisl, I. E. L. Stephens, Toward an active and stable catalyst for oxygen evolution in acidic media: Ti-stabilized MnO_2. *Adv. Energy Mater.* **5**, 1500991 (2015). doi: 10.1002/aenm.201500991
136. H. A. Hansen, V. Viswanathan, J. K. Nørskov, Unifying kinetic and thermodynamic analysis of $2e^-$ and $4e^-$ reduction of oxygen on metal surfaces. *J. Phys. Chem. C* **118**, 6706–6718 (2014). doi: 10.1021/jp4100608
137. A. Michaelides, P. Hu, A density functional theory study of hydroxyl and the intermediate in the water formation reaction on Pt. *J. Chem. Phys.* **114**, 513–519 (2001). doi: 10.1063/1.1328746
138. H. Ogasawara *et al*., Structure and bonding of water on Pt(111). *Phys. Rev. Lett.* **89**, 276102 (2002). doi: 10.1103/PhysRevLett.89.276102; pmid: 12513221
139. T. Schiros *et al*., Structure and bonding of the water-hydroxyl mixed phase on Pt(111). *J. Phys. Chem. C* **111**, 15003–15012 (2007). doi: 10.1021/jp073405f
140. H. A. Hansen, J. Rossmeisl, J. K. Nørskov, Surface Pourbaix diagrams and oxygen reduction activity of Pt, Ag and Ni(111) surfaces studied by DFT. *Phys. Chem. Chem. Phys.* **10**, 3722–3730 (2008). doi: 10.1039/b803956a; pmid: 18563233
141. D. Strmcnik *et al*., Enhanced electrocatalysis of the oxygen reduction reaction based on patterning of platinum surfaces with cyanide. *Nat. Chem.* **2**, 880–885 (2010). doi: 10.1038/nchem.771; pmid: 20861905
142. A. M. Gómez-Marín, J. M. Feliu, New insights into the oxygen reduction reaction mechanism on Pt(111): A detailed electrochemical study. *ChemSusChem* **6**, 1091–1100 (2013). doi: 10.1002/cssc.201200847; pmid: 23640868
143. A. D. Doyle, J. H. Montoya, A. Vojvodic, Improving oxygen electrochemistry through nanoscopic confinement. *ChemCatChem* **7**, 738–742 (2015). doi: 10.1002/cctc.201402864
144. A. Verdaguer-Casadevall, P. Hernandez-Fernandez, I. E. L. Stephens, I. Chorkendorff, S. Dahl, The effect of ammonia upon the electrocatalysis of hydrogen oxidation and oxygen reduction on polycrystalline platinum. *J. Power Sources* **220**, 205–210 (2012). doi: 10.1016/j.jpowsour.2012.07.141
145. B. B. Blizanac, P. N. Ross, N. M. Markovic, Oxygen electroreduction on Ag(111): The pH effect. *Electrochim. Acta* **52**, 2264–2271 (2007). doi: 10.1016/j.electacta.2006.06.047
146. J. S. Jirkovský *et al*., Single atom hot-spots at Au-Pd nanoalloys for electrocatalytic H_2O_2 production. *J. Am. Chem. Soc.* **133**, 19432–19441 (2011). doi: 10.1021/ja206477z; pmid: 22023652
147. T. P. Fellinger, F. Hasché, P. Strasser, M. Antonietti, Mesoporous nitrogen-doped carbon for the electrocatalytic synthesis of hydrogen peroxide. *J. Am. Chem. Soc.* **134**, 4072–4075 (2012). doi: 10.1021/ja300038p; pmid: 22339713
148. Y. Liu, X. Quan, X. Fan, H. Wang, S. Chen, High-yield electrosynthesis of hydrogen peroxide from oxygen reduction by hierarchically porous carbon. *Angew. Chem. Int. Ed.* **54**, 6837–6841 (2015). doi: 10.1002/anie.201502396; pmid: 25892325
149. A. Verdaguer-Casadevall *et al*., Trends in the electrochemical synthesis of H_2O_2: Enhancing activity and selectivity by electrocatalytic site engineering. *Nano Lett.* **14**, 1603–1608 (2014). doi: 10.1021/nl500037x; pmid: 24506229
150. Y. Hori, A. Murata, R. Takahashi, Formation of hydrocarbons in the electrochemical reduction of carbon dioxide at a copper electrode in aqueous solution. *J. Chem. Soc., Faraday Trans. I* **85**, 2309–2326 (1989). doi: 10.1039/f19898502309
151. Y. Hori, R. Takahashi, Y. Yoshinami, A. Murata, Electrochemical reduction of CO at a copper electrode. *J. Phys. Chem. B* **101**, 7075–7081 (1997). doi: 10.1021/jp970284i
152. K. P. Kuhl, E. R. Cave, D. N. Abram, T. F. Jaramillo, New insights into the electrochemical reduction of carbon dioxide on metallic copper surfaces. *Energy Environ. Sci.* **5**, 7050–7059 (2012). doi: 10.1039/c2ee21234j
153. A. A. Peterson, J. K. Nørskov, Activity descriptors for CO_2 electroreduction to methane on transition-metal catalysts. *J. Phys. Chem. Lett.* **3**, 251–258 (2012). doi: 10.1021/jz201461p
154. C. Shi, H. A. Hansen, A. C. Lausche, J. K. Nørskov, Trends in electrochemical CO_2 reduction activity for open and close-packed metal surfaces. *Phys. Chem. Chem. Phys.* **16**, 4720–4727 (2014). doi: 10.1039/c3cp54822h; pmid: 24468980
155. K. P. Kuhl *et al*., Electrocatalytic conversion of carbon dioxide to methane and methanol on transition metal surfaces. *J. Am. Chem. Soc.* **136**, 14107–14113 (2014). doi: 10.1021/ja505791r; pmid: 25259478
156. A. A. Peterson, F. Abild-Pedersen, F. Studt, J. Rossmeisl, J. K. Nørskov, How copper catalyzes the electroreduction of carbon dioxide into hydrocarbon fuels. *Energy Environ. Sci.* **3**, 1311–1315 (2010). doi: 10.1039/c0ee00071j

157. B. A. Rosen *et al.*, Ionic liquid-mediated selective conversion of CO_2 to CO at low overpotentials. *Science* **334**, 643–644 (2011). doi: 10.1126/science.1209786; pmid: 21960532
158. J. H. Montoya, A. A. Peterson, J. K. Nørskov, Insights into C-C coupling in CO_2 electroreduction on copper electrodes. *ChemCatChem* **5**, 737–742 (2013). doi: 10.1002/cctc.201200564
159. J. H. Montoya, C. Shi, K. Chan, J. K. Nørskov, Theoretical insights into a CO dimerization mechanism in CO_2 electroreduction. *J. Phys. Chem. Lett.* **6**, 2032–2037 (2015). doi: 10.1021/acs.jpclett.5b00722; pmid: 26266498
160. K. J. P. Schouten, Y. Kwon, C. J. M. van der Ham, Z. Qin, M. T. M. Koper, A new mechanism for the selectivity to C-1 and C-2 species in the electrochemical reduction of carbon dioxide on copper electrodes. *Chem. Sci.* **2**, 1902–1909 (2011). doi: 10.1039/c1sc00277e
161. K. J. P. Schouten, Z. Qin, E. Pérez Gallent, M. T. M. Koper, Two pathways for the formation of ethylene in CO reduction on single-crystal copper electrodes. *J. Am. Chem. Soc.* **134**, 9864–9867 (2012). doi: 10.1021/ja302668n; pmid: 22670713
162. E. Bertheussen *et al.*, Acetaldehyde as an intermediate in the electroreduction of carbon monoxide to ethanol on oxide-derived copper. *Angew. Chem. Int. Ed.* **55**, 1450–1454 (2016). doi: 10.1002/anie.201508851; pmid: 26692282
163. C. W. Li, J. Ciston, M. W. Kanan, Electroreduction of carbon monoxide to liquid fuel on oxide-derived nanocrystalline copper. *Nature* **508**, 504–507 (2014). doi: 10.1038/nature13249; pmid: 24717429
164. C. J. Pickett, J. Talarmin, Electrosynthesis of ammonia. *Nature* **317**, 652–653 (1985). doi: 10.1038/317652a0
165. G. Marnellos, M. Stoukides, Ammonia synthesis at atmospheric pressure. *Science* **282**, 98–100 (1998). doi: 10.1126/science.282.5386.98; pmid: 9756486
166. R. Lan, J. T. S. Irvine, S. Tao, Synthesis of ammonia directly from air and water at ambient temperature and pressure. *Sci. Rep.* **3**, 1145 (2013). doi: 10.1038/srep01145; pmid: 23362454
167. K. Kugler, M. Luhn, J. A. Schramm, K. Rahimi, M. Wessling, Galvanic deposition of Rh and Ru on randomly structured Ti felts for the electrochemical NH_3 synthesis. *Phys. Chem. Chem. Phys.* **17**, 3768–3782 (2015). doi: 10.1039/C4CP05501B; pmid: 25556769
168. V. Kordali, G. Kyriacou, C. Lambrou, Electrochemical synthesis of ammonia at atmospheric pressure and low temperature in a solid polymer electrolyte cell. *Chem. Commun.* **2000**, 1673–1674 (2000). doi: 10.1039/b004885m
169. E. Skúlason *et al.*, A theoretical evaluation of possible transition metal electro-catalysts for N_2 reduction. *Phys. Chem. Chem. Phys.* **14**, 1235–1245 (2012). doi: 10.1039/C1CP22271F; pmid: 22146855
170. J. H. Montoya, C. Tsai, A. Vojvodic, J. K. Nørskov, The challenge of electrochemical ammonia synthesis: A new perspective on the role of nitrogen scaling relations. *ChemSusChem* **8**, 2180–2186 (2015). doi: 10.1002/cssc.201500322; pmid: 26097211
171. Y. Abghoui *et al.*, Enabling electrochemical reduction of nitrogen to ammonia at ambient conditions through rational catalyst design. *Phys. Chem. Chem. Phys.* **17**, 4909–4918 (2015). doi: 10.1039/C4CP04838E; pmid: 25446373
172. S. Licht *et al.*, Ammonia synthesis by N_2 and steam electrolysis in molten hydroxide suspensions of nanoscale Fe_2O_3. *Science* **345**, 637–640 (2014). doi: 10.1126/science.1254234; pmid: 25104378
173. X. Hong, K. Chan, C. Tsai, J. K. Nørskov, How doped MoS_2 breaks transition-metal scaling relations for CO_2 electrochemical reduction. *ACS Catal.* **6**, 4428–4437 (2016). doi: 10.1021/acscatal.6b00619
174. N. B. Halck, V. Petrykin, P. Krtil, J. Rossmeisl, Beyond the volcano limitations in electrocatalysis—Oxygen evolution reaction. *Phys. Chem. Chem. Phys.* **16**, 13682–13688 (2014). doi: 10.1039/c4cp00571f; pmid: 24671166

ACKNOWLEDGMENTS

Supported by a grant from the Office of Basic Energy Sciences of the U.S. Department of Energy to the SUNCAT Center for Interface Science and Catalysis; Villum Foundation V-SUSTAIN grant 9455 to the Villum Center for the Science of Sustainable Fuels and Chemicals; the Institute of Materials Research and Engineering, Agency for Science, Technology and Research (A*STAR); and NSF Graduate Research Fellowship DGE-114747 (C.F.D.).

10.1126/science.aad4998

Combining theory and experiment in electrocatalysis: Insights into materials design

Zhi Wei Seh, Jakob Kibsgaard, Colin F. Dickens, Ib Chorkendorff, Jens K. Nørskov and Thomas F. Jaramillo

Science **355** (6321), eaad4998.
DOI: 10.1126/science.aad4998

Better living through water-splitting

Chemists have known how to use electricity to split water into hydrogen and oxygen for more than 200 years. Nonetheless, because the electrochemical route is inefficient, most of the hydrogen made nowadays comes from natural gas. Seh *et al.* review recent progress in electrocatalyst development to accelerate water-splitting, the reverse reactions that underlie fuel cells, and related oxygen, nitrogen, and carbon dioxide reductions. A unified theoretical framework highlights the need for catalyst design strategies that selectively stabilize distinct reaction intermediates relative to each other.

Science, this issue p. 10.1126/science.aad4998